
Gaussian Smoothing in Saliency Maps: The Stability-Fidelity Trade-Off in Neural Network Interpretability

Zhuorui Ye
Tsinghua University

Farzan Farnia
The Chinese University of Hong Kong

Abstract

Saliency maps have been widely used to interpret the decisions of neural network classifiers and discover phenomena from their learned functions. However, standard gradient-based maps are frequently observed to be highly sensitive to the randomness of training data and the stochasticity in the training process. In this work, we study the role of Gaussian smoothing in the well-known Smooth-Grad algorithm in the stability of the gradient-based maps to the randomness of training samples. We extend the algorithmic stability framework to gradient-based interpretation maps and prove bounds on the stability error of standard Simple-Grad, Integrated-Gradients, and Smooth-Grad saliency maps. Our theoretical results suggest the role of Gaussian smoothing in boosting the stability of gradient-based maps to the randomness of training settings. On the other hand, we analyze the faithfulness of the Smooth-Grad maps to the original Simple-Grad and show the lower fidelity under a more intense Gaussian smoothing. We support our theoretical results by performing several numerical experiments on standard image datasets. Our empirical results confirm our hypothesis on the fidelity-stability trade-off in the application of Gaussian smoothing to gradient-based interpretation maps.

1 INTRODUCTION

Deep learning models have attained state-of-the-art results over a wide array of supervised learning tasks including image classification (Krizhevsky et al., 2012),

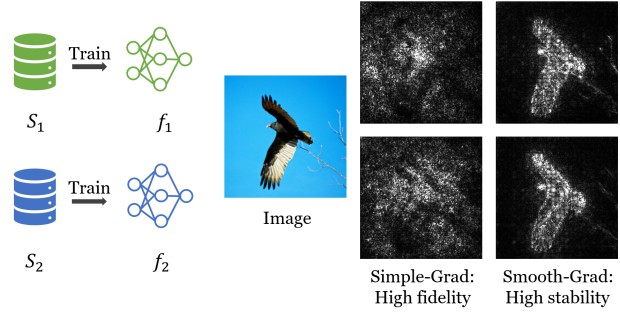


Figure 1: The stability-fidelity trade-off introduced by Gaussian smoothing. We trained neural networks on two disjoint training set splits of ImageNet, and computed the Simple-Grad and Smooth-Grad maps for the same test sample.

speech recognition (Graves et al., 2013), and text categorization (Minaee et al., 2021). The trained deep neural networks have been utilized not only to address the target classification task but also to discover the underlying rules influencing the label assignment to a feature vector. To this end, saliency maps, which highlight the features influencing the neural network’s predictions, have been widely used to gain an understanding of phenomena from data-driven models (Freiesleben et al., 2022) and further to find new discoveries and insights. For example, Mitani et al. (2020) shows the application of saliency maps to identify the region in fundus images related to anemia, and Bien et al. (2018) demonstrates that saliency maps can assist clinicians in diagnosing knee injury from MRI scans.

Specifically, gradient-based maps have been widely applied to compute saliency maps for neural net classifiers. Standard gradient-based saliency maps such as Simple-Grad (Simonyan et al., 2013) and Integrated-Gradients (Sundararajan et al., 2017), represent the input-based gradient of a neural network at a test sample, which reveals the input features with a higher local impact on the neural network classifier’s output. Therefore, the assignment of feature importance scores by a gradient-based saliency map can be utilized to reveal the main

features influencing the phenomenon.

However, a consideration for drawing conclusions from gradient-based maps is their potential sensitivity to the training algorithm of the neural network classifier. Arun et al. (2021); Woerl et al. (2023) have shown that gradient maps could be significantly different for independent yet identically distributed training sets, or for a different random initialization used for training the classifier. The sensitivity of the saliency maps is indeed valuable in debugging applications, where the map is used to identify potential reasons behind a misclassification case. On the other hand, the instability of gradient-based maps could hinder the applications of Simple-Grad and Integrated-Gradients maps for phenomena discovery (Arun et al., 2021), as for a generalizable understanding of the underlying phenomenon, the resulting saliency maps need to have limited dependence on the stochasticity of training data sampled from the underlying data distribution.

In this work, we specifically study the influence of Gaussian smoothing used in the Smooth-Grad algorithm (Smilkov et al., 2017) on the stability of a gradient-based map. We provide theoretical and numerical evidence that Gaussian smoothing could increase the stability of saliency maps to the stochasticity of the training setting, which can improve the reliability of applying the gradient-based map for phenomena understanding using the neural net classifier.

To theoretically analyze the stability properties of saliency maps, we utilize the algorithmic stability framework in Bousquet and Elisseeff (2002) to quantify the expected robustness of gradient maps to the stochasticity of a randomized training algorithm, e.g. stochastic gradient descent (SGD), and randomness of training data drawn from the underlying distribution. Following the analysis in Hardt et al. (2016), we define the stability error of a stochastic training algorithm and bound the error in terms of the number of training data and SGD training iterations for the Simple-Grad, Integrated-Gradients, and Smooth-Grad. Our stability error bounds suggest the improvement in stability by applying the randomized smoothing mechanism in Smooth-Grad. Specifically, our error bounds improve by a factor $1/\sigma$ under a standard deviation parameter σ of the Smooth-Grad’s Gaussian noise.

In addition to the stability of gradient maps under Gaussian smoothing, we also bound the faithfulness of the Gaussian smoothed saliency maps to the original Simple-Grad and Integrated-Gradients interpretation maps, for which we define fidelity error¹. We show that by increasing the standard deviation parameter

σ , the fidelity error grows proportionally to parameter σ . This relationship indicates the stabilization offered by Gaussian smoothing at the price of a higher fidelity error compared to the original saliency map. As illustrated in Figure 1, the Smooth-Grad saliency maps could be considerably more stable to the training set of the neural network, while they could significantly differ from the original Simple-Grad map. We note that different applications of saliency maps may prioritize stability or fidelity differently. For instance, debugging misclassifications would require higher fidelity, while phenomena discovery would prioritize higher stability. Therefore, understanding the stability-fidelity properties of Smooth-Grad maps helps with a principled application of the algorithm to different tasks.

We perform numerical experiments to test our theoretical results on the algorithmic stability and fidelity of interpretation maps under Gaussian smoothing. In the experiments, we tested several standard saliency maps and image datasets. We empirically analyzed a broader range of instability sources in the training setting and demonstrated that Gaussian smoothing can lead to higher stability to the changes in the training algorithm and neural network architecture. The numerical results indicate the impact of Gaussian smoothing in reducing the sensitivity of the gradient-based interpretation map to the stochasticity of the training algorithm at the cost of a higher difference from the original gradient map. We can summarize this work’s main contribution as:

- Studying the algorithmic stability and generalization properties of gradient-based saliency maps.
- Proving bounds on the algorithmic stability error of saliency maps under vanilla and noisy stochastic gradient descent (SGD) training algorithms.
- Analyzing the fidelity of Smooth-Grad maps and their faithfulness to the Simple-Grad map.
- Providing numerical evidence on the stability-fidelity trade-off of Smooth-Grad maps on standard image datasets.

2 RELATED WORK

Gradient-based Interpretation A prevalent method for generating saliency maps involves computing the gradient of a deep neural network’s output with respect to an input image. This technique is extensively utilized in numerous related studies, including Smooth-Grad (Smilkov et al., 2017), Integrated-Gradients (Sundararajan et al., 2017), DeepLIFT (Shrikumar et al., 2017), Grad-CAM (Selvaraju et al., 2017), and Grad-CAM++ (Chattpadhyay et al., 2018). However,

¹In this paper, the fidelity term refers to the faithfulness of the regularized saliency map to the original saliency map.

gradient-based saliency maps often exhibit considerable noise. To address this, various methods have been proposed to enhance the quality of these maps by reducing noise. Common strategies include altering the gradient flow through activation functions (Zeiler and Fergus, 2014; Springenberg et al., 2014), eliminating negative or minor activations (Springenberg et al., 2014; Kim et al., 2019; Ismail et al., 2021), and integrating sparsity priors (Levine et al., 2019; Zhang and Farnia, 2023). Despite these advancements, these techniques do not explicitly tackle the noise and variability in stochastic optimization and the randomness of training data.

Stability Analysis for Interpretation Maps Beyond visual quality, several studies have explored the stability of interpretation methods. Arun et al. (2021) examined the consistency within the same architecture and across different architectures for various interpretation methods on medical imaging datasets, discovering that most methods failed in their tests. Woerl et al. (2023) conducted experiments revealing that neural networks with different initializations produce distinct saliency maps. Similarly, Fel et al. (2022) highlighted the instability in interpretation maps and proposed a metric to evaluate the generalizability of these maps. To address this instability, Woerl et al. (2023) suggested a Bayesian marginalization technique to eliminate noise from random initialization and stochastic training, though it is computationally intensive due to the need to train multiple networks. Furthermore, Zhang and Farnia (2023) propose MoreauGrad which is a robust and sparsified version of the SimpleGrad and SmoothGrad algorithms. The related works (Gong et al., 2024a, 2025) develop adversarial training methods for improving the robustness and visual quality of saliency maps, while Gong et al. (2024b) leverage image super-pixels for enhanced stability. On the other hand, our work focuses on the stability effects offered by Gaussian smoothing applied in SmoothGrad.

Sanity checks for saliency maps Evaluating the application of saliency maps has been studied in several related works. The related work (Adebayo et al., 2018) proposes sanity checks for interpretation maps, where the saliency map is supposed to depend on the characteristics of input data and how the label y is determined by the input feature vector \mathbf{x} . We note that the algorithmic stability considered in our paper is orthogonal to the sanity checks designed in Adebayo et al. (2018), as the algorithmic stability analysis is performed while leaving the distribution $p_{y|\mathbf{x}}$ of training data unchanged. Similarly, the algorithmic stability notion in our work is independent of the robustness of interpretation maps to adversarial perturbations studied by Ghorbani et al. (2019) and the insensitivity of the interpretation maps to unrelated features

discussed in Kindermans et al. (2019), as our defined algorithmic stability implies neither robustness of the map to adversarially-designed perturbations nor its insensitivity to semantically unassociated features.

3 PRELIMINARIES

3.1 Supervised Learning and Neural Network Optimization

In this work, we consider a classification task with a neural network classifier. The supervised learner has access to the training set $S = \{(x_i, y_i)\}_{i=1}^n$ containing n samples, independently drawn from a population distribution $P_{X,Y}$. We use m to denote the dimension of input feature vector $x \in \mathcal{X} \subset \mathbb{R}^m$. Also, c denotes the number of classes in the classification task, i.e., $y \in \{1, 2, \dots, c\}$. We apply a gradient-based training algorithm to learn the parameters of the neural network with the training set S .

Our analysis focuses on a class of k -layer neural networks. The prediction function can be represented by $f_{\mathcal{W}}(x) = W_k \phi(W_{k-1} \phi(\dots \phi(W_1 x))) \in \mathbb{R}^c$, with \mathcal{W} denoting the vector containing all parameters. We assume $\phi(\cdot)$ is 1-Lipschitz and $\phi(0) = 0$. The neural network parameters are learned by minimizing the loss function defined over the training set, which is

$$\min_{\mathcal{W}} \frac{1}{n} \sum_{i=1}^n \ell(\mathcal{W}, x_i, y_i) \quad (1)$$

where the loss function computes the difference between prediction logits and the ground-truth label. This problem formulation is well-known as Empirical Risk Minimization (ERM). We assume our network loss function which takes as input the logit and a class label $\ell(o, y) : \mathbb{R}^c \times \mathcal{Y} \rightarrow \mathbb{R}$ to be 1-Lipschitz. The commonly used cross-entropy loss function satisfies this property.

To train the neural network's parameters, we consider the standard stochastic gradient descent (SGD) optimizer that performs T iterations of uniformly selecting a training data point (x_i, y_i) and using this rule:

$$\mathcal{W}_{t+1} = \mathcal{W}_t - \alpha_t \nabla_{\mathcal{W}} \ell(\mathcal{W}_t, x_i, y_i) \quad (2)$$

We also consider the noisy stochastic gradient descent (SGD) algorithm, with the following update rule at iteration t :

$$\begin{aligned} \mathcal{W}_{t+1} &= \mathcal{W}_t - \alpha_t \nabla_{\mathcal{W}} \tilde{\ell}(\mathcal{W}_t, x_i, y_i) \\ \text{where } \tilde{\ell}(\mathcal{W}, x, y) &:= \mathbb{E}_{\mathcal{V} \in N(0, \kappa^2 I)} [\ell(\mathcal{W} + \mathcal{V}, x, y)] \end{aligned} \quad (3)$$

In the following proposition, we show the noisy loss function optimized in the above update rule is a smooth function.

Proposition 1. Suppose that for every x, y the loss function $\ell(\mathcal{W}, x, y)$ is L -Lipschitz with respect to \mathcal{W} . Then, the noisy loss function $\tilde{\ell}(\mathcal{W}, x, y)$ is $\frac{L}{\kappa}$ -smooth with respect to \mathcal{W} .

3.2 Notations

Throughout the paper, the norm $\|\cdot\|$ refers to the ℓ_2 -norm for both vectors and matrices. We assume that the ℓ_2 -matrix norm of each weight matrix W_i is bounded by B_i , and the input image ℓ_2 -norm or $\|x\|$ is upper bounded by C . We let x_{\min} and x_{\max} denote the minimum and maximum possible values of all pixels in x , respectively. Thus, $x_{\max} - x_{\min}$ denotes the pixel value range. To simplify our formula, we use the notation $\Delta_{t,i}$ as the sum of the product of all $(t-i)$ -subsets of B_1, \dots, B_t . In particular, we define $\Delta_{t,0} = \prod_{i=1}^t B_i$, $\Delta_{t,1} = \sum_{i=1}^t \prod_{j \neq i, j \leq t} B_j$.

3.3 Saliency Maps

To interpret the classification output of a trained neural network for input x , we use the prediction logits $f_{\mathcal{W}}(x)$ and are in particular interested in the value of the y -th component, where $f_{\mathcal{W}}(x)$ is the neural network function with parameters \mathcal{W} and the input x . For the training set S , we use $\mathcal{W} = A(S)$ to denote the output of a randomized training algorithm A . Sal denotes a general saliency map algorithm, which takes $A(S)$ as input and can output a gradient-based map $\text{Sal}_{A(S)}(x, y)$ at each labeled data point (x, y) . In this work, we analyze the following standard gradient-based saliency maps:

Simple-Grad. Simple-Grad (Baehrens et al., 2010; Simonyan et al., 2013) calculates the gradient of the logit concerning each input pixel:

$$\text{SimpleGrad}_{A(S)}(x, y) = \nabla_x(f_{A(S)}(x))_y. \quad (4)$$

Smooth-Grad. Smooth-Grad (Smilkov et al., 2017) calculates the mean of the Simple-Grad map evaluated at a perturbed input data with a Gaussian noise

$$\begin{aligned} & \text{SmoothGrad}_{A(S)}(x, y) \\ &= \mathbb{E}_{z \sim N(0, \sigma^2 I)} [\nabla_x(f_{A(S)}(x + z))_y] \end{aligned} \quad (5)$$

Integrated-Gradients. Integrated-Gradients (Sundararajan et al., 2017) calculates the integral of the scaled gradient map from a reference point x_0 to the given data point x :

$$\begin{aligned} & \text{IntegratedGrad}_{A(S)}(x, y) \\ &= (x - x_0) \odot \int_0^1 \nabla_x(f_{A(S)}(x_0 + \alpha(x - x_0)))_y d\alpha. \end{aligned} \quad (6)$$

4 ALGORITHMIC STABILITY OF SALIENCY MAPS

In this work, we study the algorithmic stability of saliency maps. To this end, we first define a loss function for saliency maps

$$\ell'(A(S), x, y) = \|\text{Sal}_{A(S)}(x, y) - \text{Sal}_{A(D)}(x, y)\|, \quad (7)$$

where the reference saliency map is defined as $\text{Sal}_{A(D)}(x, y) := \mathbb{E}_{S,A}[\text{Sal}_{A(S)}(x, y)]$, the expectation of saliency maps across all training datasets S of size n drawn from the underlying data distribution D . Then we can define the corresponding test loss and training loss by

$$L'_D(A(S)) = \mathbb{E}_{(x,y) \sim D}[\ell'(A(S), x, y)] \quad (8)$$

$$L'_S(A(S)) = \mathbb{E}_{(x,y) \sim U(S)}[\ell'(A(S), x, y)] \quad (9)$$

Intuitively, a more stable saliency map algorithm to the stochasticity of training data would produce saliency maps with higher similarity for two datasets with only one different sample. Formally, we define the stability error of a saliency map algorithm Sal in the worst case as follows, where S and S' are two datasets of size n that differ in only one sample and we take the expectation over the randomness of the training algorithm A :

$$\begin{aligned} \epsilon_{\text{stability}}(\text{Sal}) := & \sup_{S, S', x, y} \mathbb{E}_A \left[\ell'(A(S), x, y) \right. \\ & \left. - \ell'(A(S'), x, y) \right] \end{aligned} \quad (10)$$

We recall the theorem stating that stability implies generalization in expectation (Bousquet and Elisseeff, 2002). In our setting, we extend the original statement and demonstrate that the generalization error of a saliency map is bounded by the stability error of the saliency map algorithm. This indicates the importance of providing theoretical guarantees for stability error.

Theorem 2. With our defined loss function, we can upper bound the generalization error of the saliency map algorithm by its stability error.

$$\mathbb{E}_{S,A}[L'_D(A(S)) - L'_S(A(S))] \leq \epsilon_{\text{stability}}(\text{Sal})$$

Proof. We defer the proof to the Appendix. \square

In this section, we then focus on the stability of some commonly used saliency map algorithms, aiming to discover what factors make a saliency map algorithm more stable.

4.1 Stability of Simple-Grad

To prove a saliency map algorithm is stable, we consider the ℓ_2 difference of the predicted saliency maps when

the two training sets S and S' only differ at one data point. To upper bound the stability error, we analyze that different loss functions of saliency maps, $\ell'(\cdot)$, are bounded and Lipschitz.

Similar to Hardt et al. (2016), we consider using the stochastic gradient descent (SGD) algorithm (can be vanilla or noisy version) and need some assumptions for the training loss function.

Assumption 3. (a) The loss function $\ell(\cdot, x, y)$ is L -Lipschitz for all x, y , that is, for any \mathcal{V}, \mathcal{W} we have

$$\|\ell(\mathcal{V}, x, y) - \ell(\mathcal{W}, x, y)\| \leq L\|\mathcal{V} - \mathcal{W}\|$$

(b) The loss function $\ell(\cdot, x, y)$ is β -smooth for all x, y , that is, for any \mathcal{V}, \mathcal{W} we have

$$\|\nabla_{\mathcal{V}}\ell(\mathcal{V}, x, y) - \nabla_{\mathcal{W}}\ell(\mathcal{W}, x, y)\| \leq \beta\|\mathcal{V} - \mathcal{W}\|$$

Remark 4. (1) For noisy SGD introduced in Equation 3, we can upper bound $L \leq \Delta_{k,1}C$ due to lemma D.8, and upper bound $\beta \leq \frac{L}{\kappa}$ according to Proposition 1.

(2) For regular SGD, the upper bound for L still holds. However, based on lemma D.8, we need to additionally assume both the activation function $\phi(\cdot)$ and the loss function which takes as input the logit $\ell(\cdot, y)$ for any y are 1-smooth to show $\beta \leq (3k + 1)\Delta_{k,1}^2C^2$.

The following theorem upper bounds the stability error of Simple-Grad in terms of parameters of the SGD algorithm (T and c), the Lipschitz and smoothness constants of the loss function (L and β), and the quantity related to the neural network (Γ). Here we refer to both the vanilla and noisy versions as the SGD algorithm.

Theorem 5. Suppose Assumption 3(a) and 3(b) hold. If we run SGD for T steps with a decaying step size $\alpha_t \leq c/t$ in iteration t , by defining $\Gamma = (2\Delta_{k,0} \sum_{i=1}^{k-1} \Delta_{i,1}C)^{1/(\beta c+1)}(2\Delta_{k,0})^{\beta c/(\beta c+1)}$, we can bound the stability error of Simple-Grad by

$$\begin{aligned} \epsilon_{\text{stability}}(\text{SimpleGrad}) &\leq \text{Up}(\text{SimpleGrad}) \\ &:= \frac{1 + \beta c}{n - 1} (2cL)^{\frac{1}{\beta c+1}} T^{\frac{\beta c}{\beta c+1}} \Gamma \end{aligned}$$

Proof. We defer the proof to the Appendix. \square

4.2 Stability of Smooth-Grad

For Smooth-Grad with a simple adjustment where we perform normalization to ensure the input to the neural network has an ℓ_2 norm not exceeding C , we can prove the following upper bound.

Theorem 6. Suppose Assumption 3(a) and 3(b) hold. If we run SGD for T steps with a decaying step size

$\alpha_t \leq c/t$ in iteration t , we can bound the stability error of Smooth-Grad by

$$\begin{aligned} \epsilon_{\text{stability}}(\text{SmoothGrad}) &\leq \text{Up}(\text{SimpleGrad}) \\ &\times \left(\frac{\Delta_{k,1}}{2\sigma\Delta_{k,0} \sum_{i=1}^{k-1} \Delta_{i,1}} \right)^{\frac{1}{\beta c+1}} \end{aligned}$$

Proof. We defer the proof to the Appendix. \square

Comparing Theorem 5 and Theorem 6, we observe that Smooth-Grad exhibits a lower stability error by multiplying a dimension-free constant smaller than 1. Theorem 6 also provides a non-asymptotic dimension-free guarantee that as the σ value becomes larger, the stability error vanishes to 0. This suggests that the smoothing filter enhances the algorithmic stability of high-dimensional saliency maps.

4.3 Fidelity of Gaussian Smoothed Saliency Maps

We then illustrate that this stability improvement comes at the expense of fidelity. As σ increases, the Gaussian-smoothed saliency map diverges further from the ground-truth map.

First, we formally define the fidelity error $\epsilon_{\text{fidelity}}(\text{Sal}, \sigma)$ of the σ -smoothed saliency map algorithm Sal as the largest possible expected ℓ_2 -distance between the smoothed and unsmoothed saliency maps for any training set S , labeled data sample x, y , where the expectation is over the randomness of the algorithm. Specifically, fidelity error is defined as:

$$\begin{aligned} \sup_{S, x, y} \mathbb{E}_A &\left[\left\| \mathbb{E}_{z \sim N(0, \sigma^2 I)} [\text{Sal}_{A(S)}(x + z, y)] \right. \right. \\ &\quad \left. \left. - \text{Sal}_{A(S)}(x, y) \right\| \right] \end{aligned} \quad (11)$$

We present the following proposition to upper bound the fidelity error of Smooth-Grad and the smoothed version of Integrated-Grad, indicating the fidelity error grows with the Gaussian smooth factor σ .

Proposition 7. The fidelity error of both Smooth-Grad and the smoothed version of Integrated-Grad increase accordingly with the Gaussian smoothing factor σ . In particular, by defining $\Lambda = \Delta_{k,0} \sum_{i=1}^{k-1} \Delta_{i,0}$, we have

$$\begin{aligned} \epsilon_{\text{fidelity}}(\text{SimpleGrad}, \sigma) &\leq \Lambda\sigma\sqrt{m} \\ \epsilon_{\text{fidelity}}(\text{IntegratedGrad}, \sigma) &\leq \Lambda(3C + 1)\sigma\sqrt{m} \end{aligned}$$

Proof. We defer the proof to the Appendix. \square

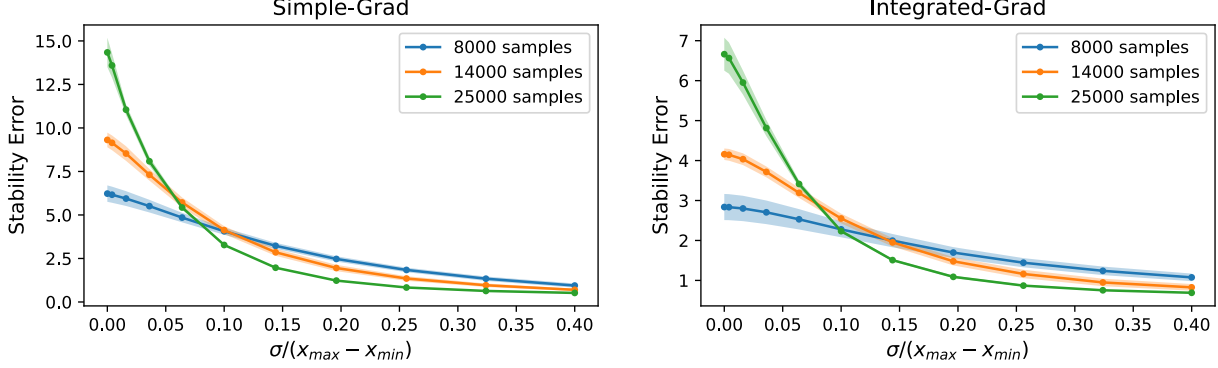


Figure 2: Relationship between stability error of saliency maps and sigma, evaluated on the CIFAR10 test set. The shaded region indicates one standard deviation from the mean value. Here noise level $x_{\max} - x_{\min}$ represents the largest value range for all pixels, following the practice of Smilkov et al. (2017).

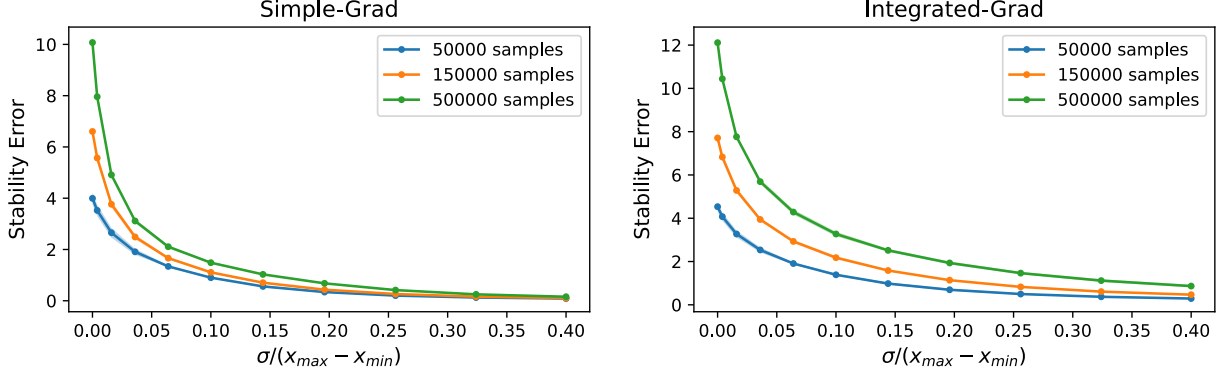


Figure 3: Relationship between stability error of saliency maps and sigma, evaluated on the ImageNet test set. The shaded region indicates one standard deviation from the mean value.

5 NUMERICAL EXPERIMENTS

The goal of our numerical experiments is to validate the stability-fidelity tradeoff incurred by choosing different smoothing factors σ . We evaluated different neural network architectures and different training set sizes on CIFAR10 (Krizhevsky and Hinton, 2009) and ImageNet (Deng et al., 2009) datasets. We trained ResNet34 (He et al., 2015) for CIFAR10 and ResNet50 for ImageNet, due to different dataset scales. More detailed experiment configurations are in Appendix C.

5.1 Saliency Map Stability and Fidelity Numerical Results

To evaluate the algorithmic stability of saliency maps, we need to perturb one training sample multiple times and train a neural network from scratch for each perturbed training set S' . However, this approach is computationally prohibitive. As an alternative, we randomly divide the original training set S into two disjoint subsets S_1 and S_2 so that the two training sub-

sets can be regarded as independently sampled from the test distribution, and train two neural networks $A(S_1)$ and $A(S_2)$ on them. We then use the average ℓ_2 -difference between two predicted saliency maps as a proxy for stability error, formulated as

$$\mathbb{E}_{(x,y) \sim D} \|\text{Sal}_{A(S_1)}(x, y) - \text{Sal}_{A(S_2)}(x, y)\| \quad (12)$$

We conducted experiments on CIFAR10 in Figure 2 and ImageNet in Figure 3 for different saliency map algorithms as the smoothing factor σ changes. Our results confirm that increasing σ consistently decreases the stability error of the saliency maps.

To evaluate the fidelity error of a σ -smoothed saliency map, we similarly calculate

$$\mathbb{E}_{(x,y) \sim D} \mathbb{E}_{i=1}^2 \|\mathbb{E}_{z \sim N(0, \sigma^2 I)} [\text{Sal}_{A(S_i)}(x + z, y)] - \text{Sal}_{A(S_i)}(x, y)\| \quad (13)$$

as a proxy, where $\text{Sal}_{A(S)}(x, y)$ represents a non-smoothed saliency map.

We also performed experiments on CIFAR10 in Figure 4 and ImageNet in Figure 5 to evaluate the fidelity of

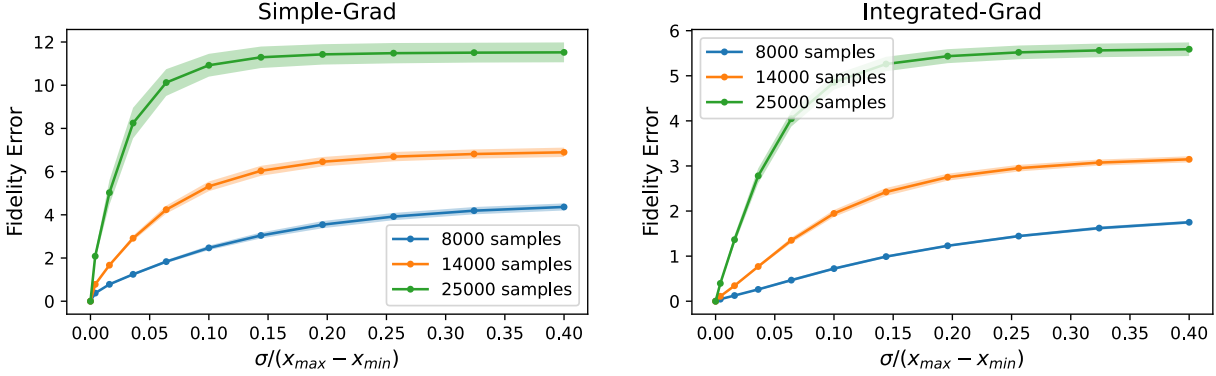


Figure 4: The relation between the saliency map fidelity error and sigma. This experiment is conducted on the test set of CIFAR10. The shaded area represents one standard deviation.

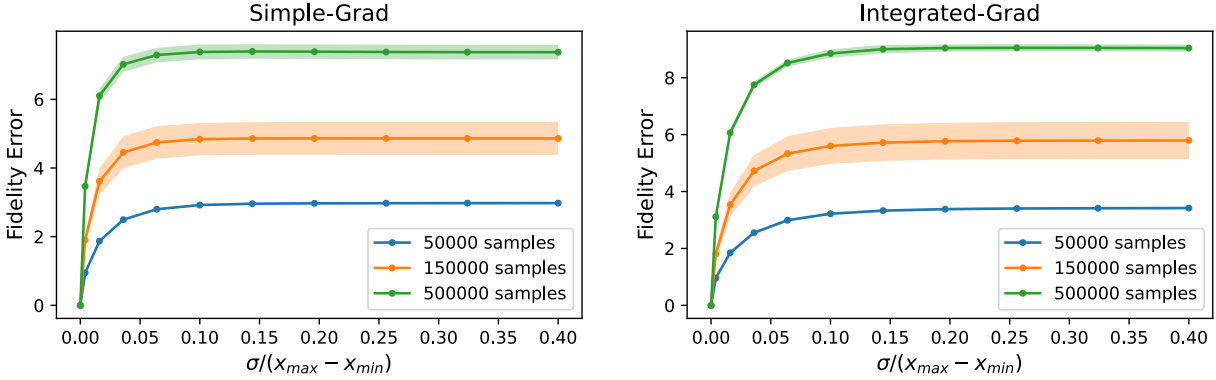


Figure 5: The relation between the saliency map fidelity error and sigma. This experiment is conducted on the test set of ImageNet. The shaded area represents one standard deviation.

the saliency maps for different saliency map algorithms as the smoothing factor σ varies. The results show that the fidelity error increases consistently as σ increases, supporting our theoretical findings.

5.2 Visualizations of Saliency Map Stability and Fidelity

We visualize the differences between two saliency maps when training two neural networks on different training sets. From the results of two neural networks trained on disjoint training subsets of 500,000 samples from ImageNet in Figure 7, we observe that Gaussian smoothing makes the saliency maps more similar and thus more stable to the randomness of training samples.

Additionally, we visualize the trend that a larger σ results in a smoothed saliency map that is less similar to the vanilla version, as demonstrated in Figure 8 for Simple-Grad and in Figure 9 for Integrated-Grad.

The visualization results, along with our theoretical findings, indicate that Gaussian smoothing enhances the stability of saliency maps at the expense of fi-

dentity. Therefore, the choice of σ in practical applications should be carefully determined by considering this trade-off, since applications of saliency maps could require different levels of the two factors.

5.3 Empirical Results on Generalized Settings

Beyond the randomness of training settings, we further examine other sources that could cause instability in interpretation: different training recipes and model architectures. Extensive experiments across various settings, as shown in Table 1, empirically indicate that the stabilizing effect of Gaussian smoothing also holds in different scenarios. We use the structural similarity index measure SSIM (Wang et al., 2004) to evaluate the similarity of two saliency maps and a larger SSIM value indicates that the two maps are more perceptually similar. We additionally use top-k mIoU to evaluate the similarity by calculating mIoU between the most salient $k = 500$ pixels of two maps.

In the top four rows, we train two ResNet50 models on two disjoint ImageNet training subsets of 500,000

Table 1: Average SSIM and top-k mIoU scores for saliency maps from two neural networks evaluated on a random subset of the ImageNet test set. Smoothed scores are computed after applying Gaussian smoothing to both saliency maps. We consider various settings including different training sets (DT), different recipes for training (DR), different architectures of neural networks (DA). We use $\sigma/(x_{\max} - x_{\min}) = 0.15$ and draw 100 samples to calculate smoothed saliency maps in all settings. **Bold** represents the better score.

Setting	Algorithm	Architecture	SSIM	Smoothed SSIM	top-k mIoU	Smoothed top-k mIoU
DT	Simple-Grad	ResNet50	0.163	0.227	0.061	0.122
DT	Integrated-Grad	ResNet50	0.270	0.326	0.085	0.163
DT	Grad-CAM	ResNet50	0.872	0.846	0.110	0.158
DT	Grad-CAM++	ResNet50	0.874	0.886	0.127	0.221
DR	Simple-Grad	ResNet50	0.150	0.179	0.050	0.092
DR	Integrated-Grad	ResNet50	0.259	0.294	0.072	0.141
DR	Grad-CAM	ResNet50	0.729	0.754	0.070	0.165
DR	Grad-CAM++	ResNet50	0.725	0.743	0.047	0.174
DA	Simple-Grad	ResNet34 & ResNet50	0.141	0.180	0.053	0.112
DA	Integrated-Grad	ResNet34 & ResNet50	0.249	0.279	0.064	0.150
DA	Simple-Grad	ResNet50 & Swin-T	0.095	0.140	0.025	0.068
DA	Integrated-Grad	ResNet50 & Swin-T	0.172	0.202	0.031	0.088
DA	Simple-Grad	ResNet50 & ConvNeXt-T	0.102	0.167	0.035	0.079
DA	Integrated-Grad	ResNet50 & ConvNeXt-T	0.208	0.258	0.041	0.109
DA	Simple-Grad	Swin-T & ConvNeXt-T	0.201	0.201	0.047	0.100
DA	Integrated-Grad	Swin-T & ConvNeXt-T	0.268	0.242	0.053	0.121

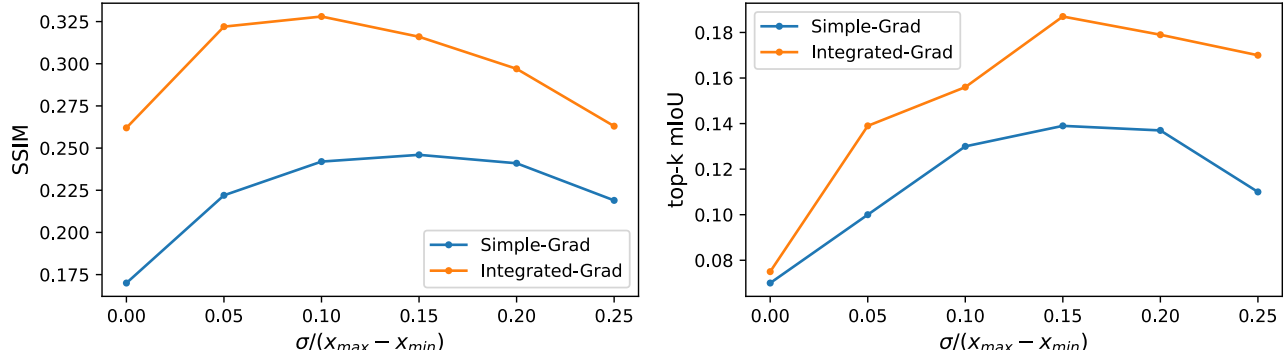


Figure 6: The effect of Gaussian smoothing with different σ choices on SSIM and top-k mIoU for Simple-Grad and Integrated-Grad, where the two neural networks are trained on two splits of the ImageNet training set.

samples each. For all other rows, we use pre-trained checkpoints provided by TorchVision (maintainers and contributors, 2016). Since TorchVision provides two ResNet50 checkpoints trained with different schemes, we use this pair for the middle four rows of our table. For the ResNet50 models in the bottom rows, we use the checkpoint **version 1**.

First, when networks are trained on different training sets, Gaussian smoothing makes the resulting saliency maps more similar for both Simple-Grad and Integrated-Grad. For advanced saliency map algorithms such as Grad-CAM (Selvaraju et al., 2017) and Grad-CAM++ (Chattopadhyay et al., 2018), the vanilla maps have high SSIM values due to the concentrated and block-like patterns, yet their top-k mIoU are still modest. Applying Gaussian smoothing occasionally causes significant visual changes in one saliency map

but not the other, resulting in a slightly lower SSIM value for Grad-CAM. Second, the instability caused by different training recipes can be largely mitigated by Gaussian smoothing, with better SSIM and top-k mIoU scores. See the corresponding visualization for Simple-Grad in Figure 10 in Appendix A.

Third, the effect of smoothing holds for most cross-architecture experiments. Besides ResNet, we also evaluated more recent architectures such as Swin Transformer (Liu et al., 2021) and ConvNeXt (Liu et al., 2022). See Figures 11, 12, and 16 for corresponding visualizations in Appendix A. Finally, saliency map algorithms like Grad-CAM and Grad-CAM++ also enjoy improved stability through Gaussian smoothing in some scenarios according to Table 1. See Figures 13, 14, and 15 for visualizations of Integrated-Grad, Grad-CAM, and Grad-CAM++ in Appendix A. Figure 6

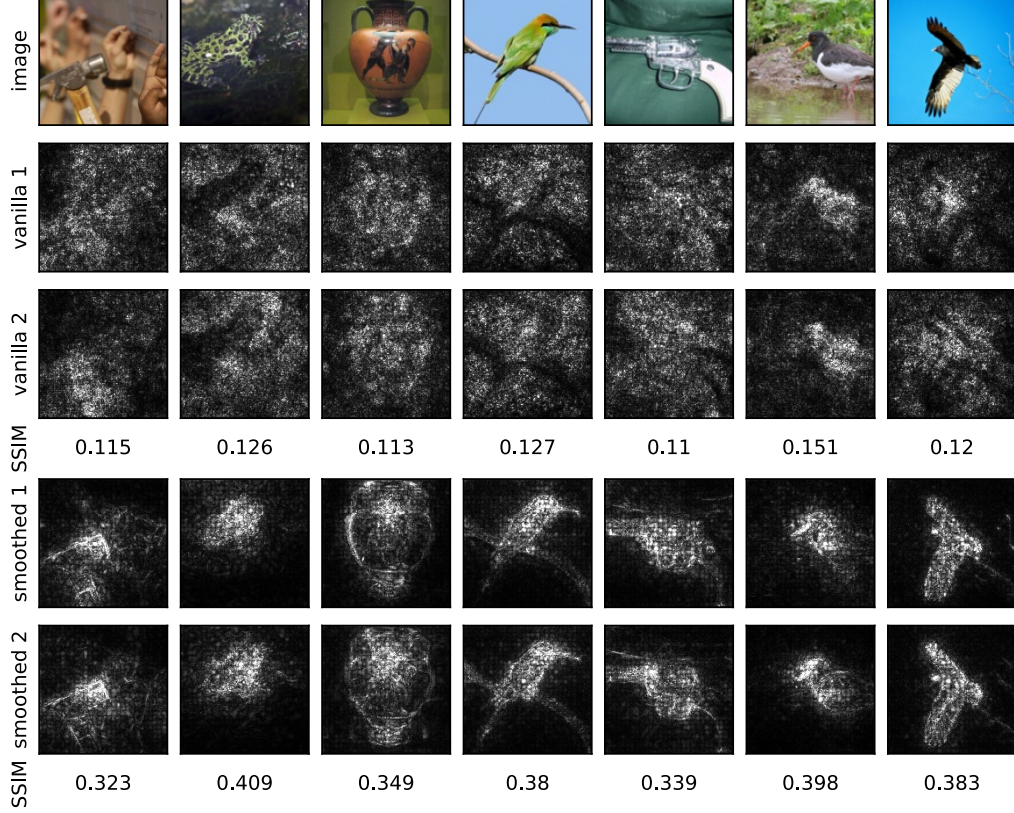


Figure 7: Visualization of saliency map differences for two ResNet50 models trained on disjoint subsets of the ImageNet training set, each containing 500,000 random samples. The first row shows the input image. The second and third rows display the Simple-Grad results. The fourth and fifth rows show the Smooth-Grad results with $\sigma/(x_{\max} - x_{\min}) = 0.15$.

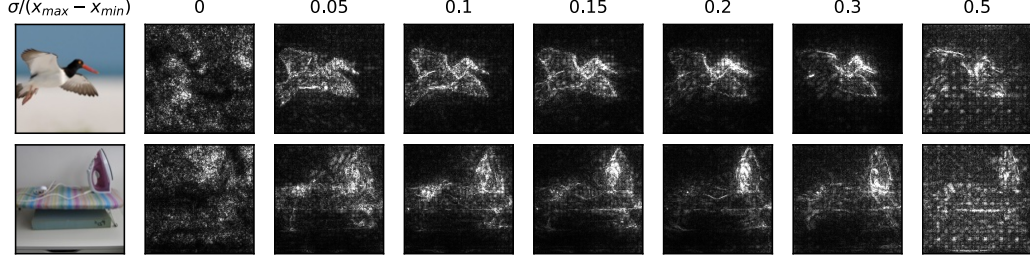


Figure 8: Visualization of Simple-Grad becoming less similar to the original unsmoothed map with the Gaussian smoothing as the factor $\sigma/(x_{\max} - x_{\min})$ increases.

shows that the highest stabilizing effect of Gaussian smoothing can be achieved with a proper choice of σ .

6 CONCLUSION

In this work, we analyzed the stability fidelity trade-off in the widely-used Smooth-Grad interpretation map. Our results indicate the impact of Gaussian smoothing on the stability of saliency maps to the stochasticity of the training setting. On the other hand, we show Gaussian smoothing could lead to a higher discrepancy

with the original gradient map. Therefore, Gaussian smoothing needs to be utilized properly, depending on the target application's aimed stability and fidelity scores. Performing an analytical study of the effects of Gaussian smoothing on the sanity checks in Adebayo et al. (2018) is an interesting future direction to our work. While Adebayo et al. (2018) numerically shows that Smooth-Grad passes the sanity checks, an analysis of the σ parameter in Gaussian smoothing and Smooth-Grad's performance in the sanity checks will be a relevant topic for future study.

Acknowledgments

The work of Farzan Farnia is partially supported by a grant from the Research Grants Council of the Hong Kong Special Administrative Region, China, Project 14209920, and is partially supported by CUHK Direct Research Grants with CUHK Project No. 4055164 and 4937054. Also, the authors would like to thank the anonymous reviewers for their constructive feedback and suggestions.

References

- Adebayo, J., Gilmer, J., Muelly, M., Goodfellow, I., Hardt, M., and Kim, B. (2018). Sanity checks for saliency maps. *Advances in neural information processing systems*, 31.
- Arun, N., Gaw, N., Singh, P., Chang, K., Aggarwal, M., Chen, B., Hoebel, K., Gupta, S., Patel, J., Gidwani, M., et al. (2021). Assessing the trustworthiness of saliency maps for localizing abnormalities in medical imaging. *Radiology: Artificial Intelligence*, 3(6):e200267.
- Baehrens, D., Schroeter, T., Harmeling, S., Kawanabe, M., Hansen, K., and Müller, K.-R. (2010). How to explain individual classification decisions. *The Journal of Machine Learning Research*, 11:1803–1831.
- Bien, N., Rajpurkar, P., Ball, R. L., Irvin, J., Park, A., Jones, E., Bereket, M., Patel, B. N., Yeom, K. W., Shpanskaya, K., et al. (2018). Deep-learning-assisted diagnosis for knee magnetic resonance imaging: development and retrospective validation of mrnet. *PLoS medicine*, 15(11):e1002699.
- Bousquet, O. and Elisseeff, A. (2002). Stability and generalization. *The Journal of Machine Learning Research*, 2:499–526.
- Chattopadhyay, A., Sarkar, A., Howlader, P., and Balasubramanian, V. N. (2018). Grad-cam++: Generalized gradient-based visual explanations for deep convolutional networks. In *2018 IEEE winter conference on applications of computer vision (WACV)*, pages 839–847. IEEE.
- Deng, J., Dong, W., Socher, R., Li, L.-J., Li, K., and Fei-Fei, L. (2009). Imagenet: A large-scale hierarchical image database. In *2009 IEEE Conference on Computer Vision and Pattern Recognition*, pages 248–255.
- Fel, T., Vigouroux, D., Cadène, R., and Serre, T. (2022). How good is your explanation? algorithmic stability measures to assess the quality of explanations for deep neural networks. In *Proceedings of the IEEE/CVF Winter Conference on Applications of Computer Vision*, pages 720–730.
- Freiesleben, T., König, G., Molnar, C., and Tejero-Cantero, A. (2022). Scientific inference with interpretable machine learning: Analyzing models to learn about real-world phenomena. *arXiv preprint arXiv:2206.05487*.
- Ghorbani, A., Abid, A., and Zou, J. (2019). Interpretation of neural networks is fragile. In *Proceedings of the AAAI conference on artificial intelligence*, volume 33, pages 3681–3688.
- Gildenblat, J. and contributors (2021). Pytorch library for cam methods. <https://github.com/jacobgil/pytorch-cam>.
- Gong, S., Dou, Q., and Farnia, F. (2024a). Structured gradient-based interpretations via norm-regularized adversarial training. In *Proceedings of the IEEE/CVF Conference on Computer Vision and Pattern Recognition*, pages 11009–11018.
- Gong, S., Haoyu, L., Dou, Q., and Farnia, F. (2025). Boosting the visual interpretability of clip via adversarial fine-tuning. In *The Thirteenth International Conference on Learning Representations*.
- Gong, S., Zhang, J., Dou, Q., and Farnia, F. (2024b). A super-pixel-based approach to the stable interpretation of neural networks. *arXiv preprint arXiv:2412.14509*.
- Graves, A., Mohamed, A.-r., and Hinton, G. (2013). Speech recognition with deep recurrent neural networks. In *2013 IEEE international conference on acoustics, speech and signal processing*, pages 6645–6649. Ieee.
- Hardt, M., Recht, B., and Singer, Y. (2016). Train faster, generalize better: Stability of stochastic gradient descent. In *International conference on machine learning*, pages 1225–1234. PMLR.
- He, K., Zhang, X., Ren, S., and Sun, J. (2015). Deep residual learning for image recognition.
- Ismail, A. A., Corrada Bravo, H., and Feizi, S. (2021). Improving deep learning interpretability by saliency guided training. *Advances in Neural Information Processing Systems*, 34:26726–26739.
- Kim, B., Seo, J., Jeon, S., Koo, J., Choe, J., and Jeon, T. (2019). Why are saliency maps noisy? cause of and solution to noisy saliency maps. In *2019 IEEE/CVF International Conference on Computer Vision Workshop (ICCVW)*, pages 4149–4157. IEEE.
- Kindermans, P.-J., Hooker, S., Adebayo, J., Alber, M., Schütt, K. T., Dähne, S., Erhan, D., and Kim, B. (2019). The (un)reliability of saliency methods. *Explainable AI: Interpreting, explaining and visualizing deep learning*, pages 267–280.
- Krizhevsky, A. and Hinton, G. (2009). Learning multiple layers of features from tiny images. *Master’s*

- thesis, Department of Computer Science, University of Toronto.*
- Krizhevsky, A., Sutskever, I., and Hinton, G. E. (2012). Imagenet classification with deep convolutional neural networks. *Advances in neural information processing systems*, 25.
- Levine, A., Singla, S., and Feizi, S. (2019). Certifiably robust interpretation in deep learning. *arXiv preprint arXiv:1905.12105*.
- Lin, W., Khan, M. E., and Schmidt, M. (2019). Stein’s lemma for the reparameterization trick with exponential family mixtures.
- Liu, Z., Lin, Y., Cao, Y., Hu, H., Wei, Y., Zhang, Z., Lin, S., and Guo, B. (2021). Swin transformer: Hierarchical vision transformer using shifted windows. In *Proceedings of the IEEE/CVF International Conference on Computer Vision (ICCV)*.
- Liu, Z., Mao, H., Wu, C.-Y., Feichtenhofer, C., Darrell, T., and Xie, S. (2022). A convnet for the 2020s. *Proceedings of the IEEE/CVF Conference on Computer Vision and Pattern Recognition (CVPR)*.
- maintainers, T. and contributors (2016). Torchvision: Pytorch’s computer vision library. <https://github.com/pytorch/vision>.
- Minaee, S., Kalchbrenner, N., Cambria, E., Nikzad, N., Chenaghlu, M., and Gao, J. (2021). Deep learning-based text classification: a comprehensive review. *ACM computing surveys (CSUR)*, 54(3):1–40.
- Mitani, A., Huang, A., Venugopalan, S., Corrado, G. S., Peng, L., Webster, D. R., Hammel, N., Liu, Y., and Varadarajan, A. V. (2020). Detection of anaemia from retinal fundus images via deep learning. *Nature Biomedical Engineering*, 4(1):18–27.
- Nesterov, Y. (2014). *Introductory Lectures on Convex Optimization: A Basic Course*. Springer Publishing Company, Incorporated, 1 edition.
- Selvaraju, R. R., Cogswell, M., Das, A., Vedantam, R., Parikh, D., and Batra, D. (2017). Grad-cam: Visual explanations from deep networks via gradient-based localization. In *Proceedings of the IEEE international conference on computer vision*, pages 618–626.
- Shrikumar, A., Greenside, P., and Kundaje, A. (2017). Learning important features through propagating activation differences. In *International conference on machine learning*, pages 3145–3153. PMLR.
- Simonyan, K., Vedaldi, A., and Zisserman, A. (2013). Deep inside convolutional networks: Visualising image classification models and saliency maps. *arXiv preprint arXiv:1312.6034*.
- Smilkov, D., Thorat, N., Kim, B., Viégas, F., and Wattenberg, M. (2017). Smoothgrad: removing noise by adding noise. *arXiv preprint arXiv:1706.03825*.
- Springenberg, J. T., Dosovitskiy, A., Brox, T., and Riedmiller, M. (2014). Striving for simplicity: The all convolutional net. *arXiv preprint arXiv:1412.6806*.
- Sundararajan, M., Taly, A., and Yan, Q. (2017). Axiomatic attribution for deep networks. In *International conference on machine learning*, pages 3319–3328. PMLR.
- Wang, Z., Bovik, A. C., Sheikh, H. R., and Simoncelli, E. P. (2004). Image quality assessment: from error visibility to structural similarity. *IEEE transactions on image processing*, 13(4):600–612.
- Woerl, A.-C., Disselhoff, J., and Wand, M. (2023). Initialization noise in image gradients and saliency maps. In *Proceedings of the IEEE/CVF Conference on Computer Vision and Pattern Recognition*, pages 1766–1775.
- Zeiler, M. D. and Fergus, R. (2014). Visualizing and understanding convolutional networks. In *Computer Vision–ECCV 2014: 13th European Conference, Zurich, Switzerland, September 6–12, 2014, Proceedings, Part I 13*, pages 818–833. Springer.
- Zhang, J. and Farnia, F. (2023). Moreaugrad: Sparse and robust interpretation of neural networks via moreau envelope. *arXiv preprint arXiv:2302.05294*.

Checklist

1. For all models and algorithms presented, check if you include:
 - (a) A clear description of the mathematical setting, assumptions, algorithm, and/or model. [Yes]
 - (b) An analysis of the properties and complexity (time, space, sample size) of any algorithm. [Yes]
 - (c) (Optional) Anonymized source code, with specification of all dependencies, including external libraries. [No]
2. For any theoretical claim, check if you include:
 - (a) Statements of the full set of assumptions of all theoretical results. [Yes]
 - (b) Complete proofs of all theoretical results. [Yes]
 - (c) Clear explanations of any assumptions. [Yes]
3. For all figures and tables that present empirical results, check if you include:
 - (a) The code, data, and instructions needed to reproduce the main experimental results (either in the supplemental material or as a URL). [Yes]

- (b) All the training details (e.g., data splits, hyperparameters, how they were chosen). [Yes]
 - (c) A clear definition of the specific measure or statistics and error bars (e.g., with respect to the random seed after running experiments multiple times). [Yes]
 - (d) A description of the computing infrastructure used. (e.g., type of GPUs, internal cluster, or cloud provider). [Yes]
4. If you are using existing assets (e.g., code, data, models) or curating/releasing new assets, check if you include:
- (a) Citations of the creator If your work uses existing assets. [Yes]
 - (b) The license information of the assets, if applicable. [Not Applicable]
 - (c) New assets either in the supplemental material or as a URL, if applicable. [Not Applicable]
 - (d) Information about consent from data providers/curators. [Not Applicable]
 - (e) Discussion of sensible content if applicable, e.g., personally identifiable information or offensive content. [Not Applicable]
5. If you used crowdsourcing or conducted research with human subjects, check if you include:
- (a) The full text of instructions given to participants and screenshots. [Not Applicable]
 - (b) Descriptions of potential participant risks, with links to Institutional Review Board (IRB) approvals if applicable. [Not Applicable]
 - (c) The estimated hourly wage paid to participants and the total amount spent on participant compensation. [Not Applicable]

A More Results

Due to the space limit of the main text, we put more results here. Figure 9 visualizes the trend of less faithfulness to the original saliency map with increasing σ . Figure 10 displays two ResNet50 checkpoints trained with different recipes. Figure 11, 12, 16 show our findings extend to the case where two neural networks use different architectures (and naturally the training recipes also differ). Figure 13, 14, 15 shows the stabilizing effect of Gaussian smoothing for Integrated-Grad, Grad-CAM, and Grad-CAM++, respectively. These visualizations, together with Table 1 in the main text, provide empirical evidence that Gaussian smoothing can generally stabilize saliency maps across various settings.

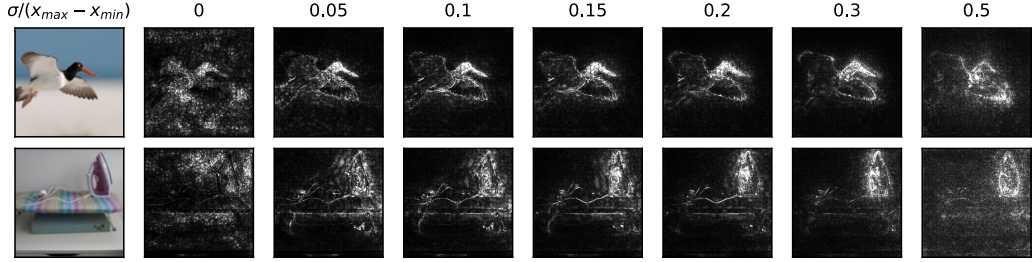


Figure 9: Visualization of Integrated-Grad becoming less similar to the original unsmeared map with the Gaussian smoothing as the factor σ increases.

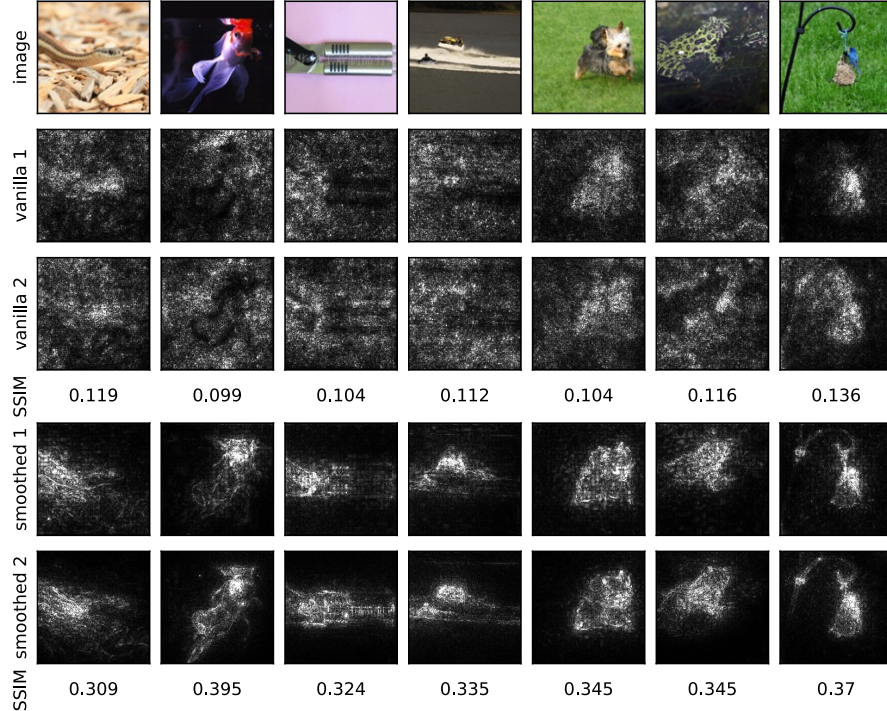


Figure 10: Visualization of saliency maps of two pre-trained ResNet50 checkpoints provided by TorchVision (maintainers and contributors, 2016). The first row is the input image. The second and third rows are Simple-Grad results. The fourth and fifth rows are Smooth-Grad with $\sigma/(x_{\max} - x_{\min}) = 0.15$.

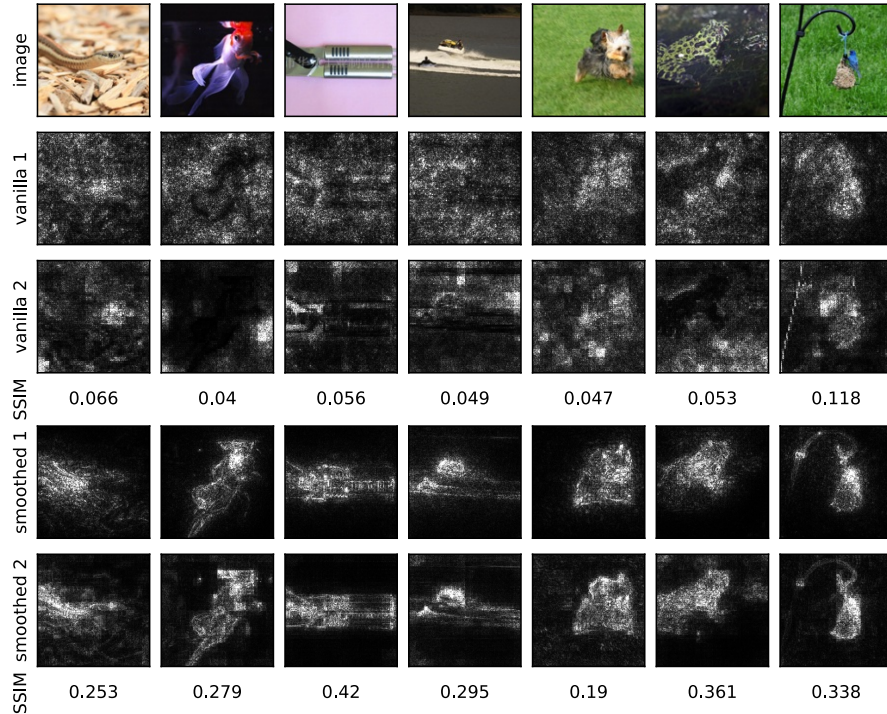


Figure 11: Visualization of saliency maps of pre-trained ResNet50 and Swin-T checkpoints provided by TorchVision (maintainers and contributors, 2016). The first row is the input image. The second and third rows are Simple-Grad results. The fourth and fifth rows are Smooth-Grad with $\sigma/(x_{\max} - x_{\min}) = 0.15$.

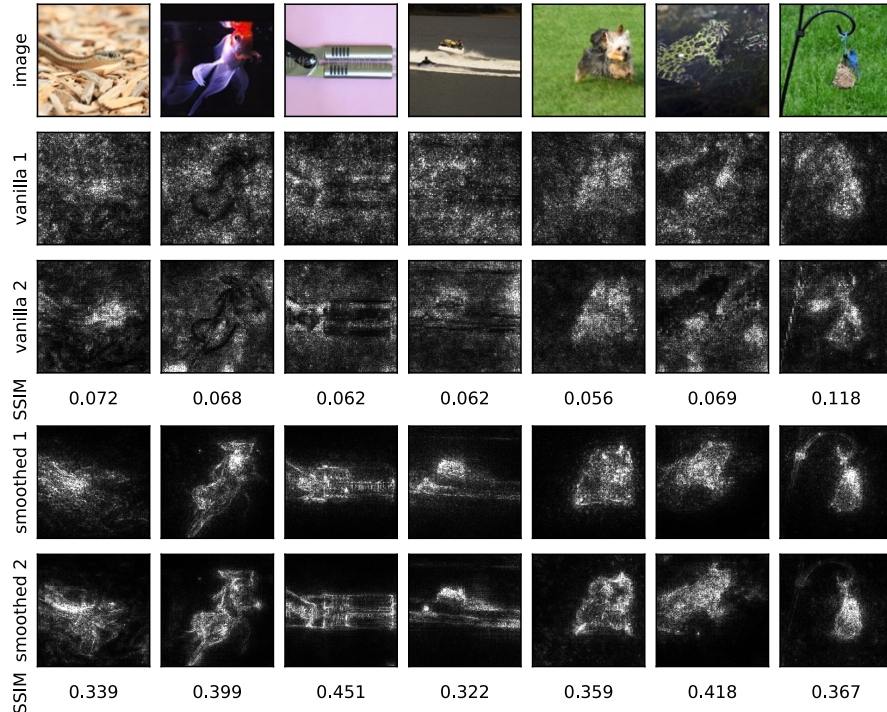


Figure 12: Visualization of saliency maps differences of pre-trained ResNet50 and ConvNeXt-tiny checkpoints provided by TorchVision (maintainers and contributors, 2016). The first row is the input image. The second and third rows are Simple-Grad results. The fourth and fifth rows are Smooth-Grad with $\sigma/(x_{\max} - x_{\min}) = 0.15$.

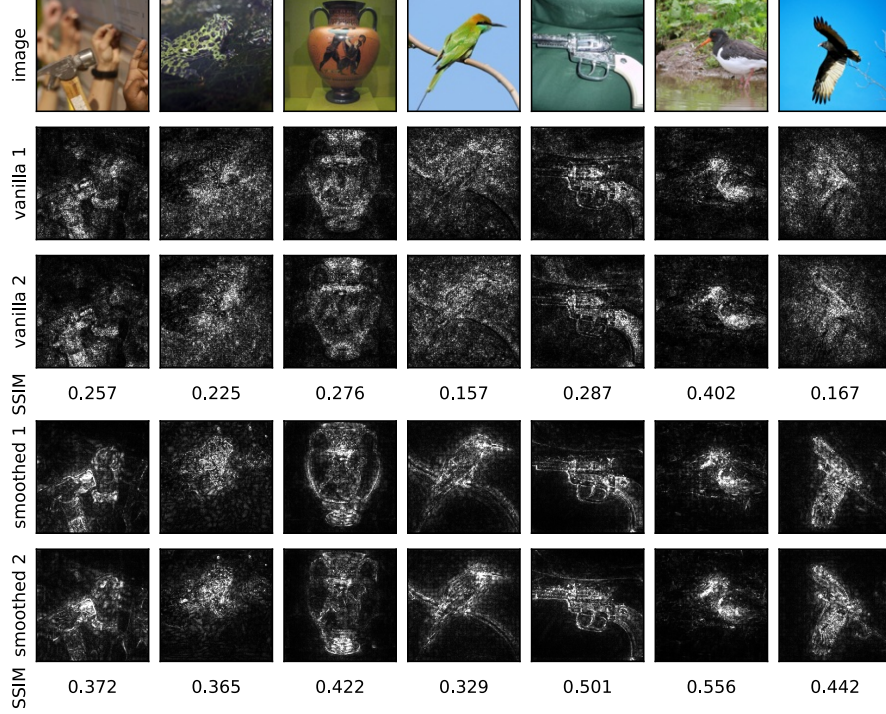


Figure 13: Visualization of Integrated-Grad and smoothed Integrated-Grad differences of two ResNet50’s trained using two disjoint halves of the training set, each with 500000 random samples. The first row is the input image. The second and third rows are Integrated-Grad results. The fourth and fifth rows are smoothed Integrated-Grad with $\sigma/(x_{\max} - x_{\min}) = 0.15$.

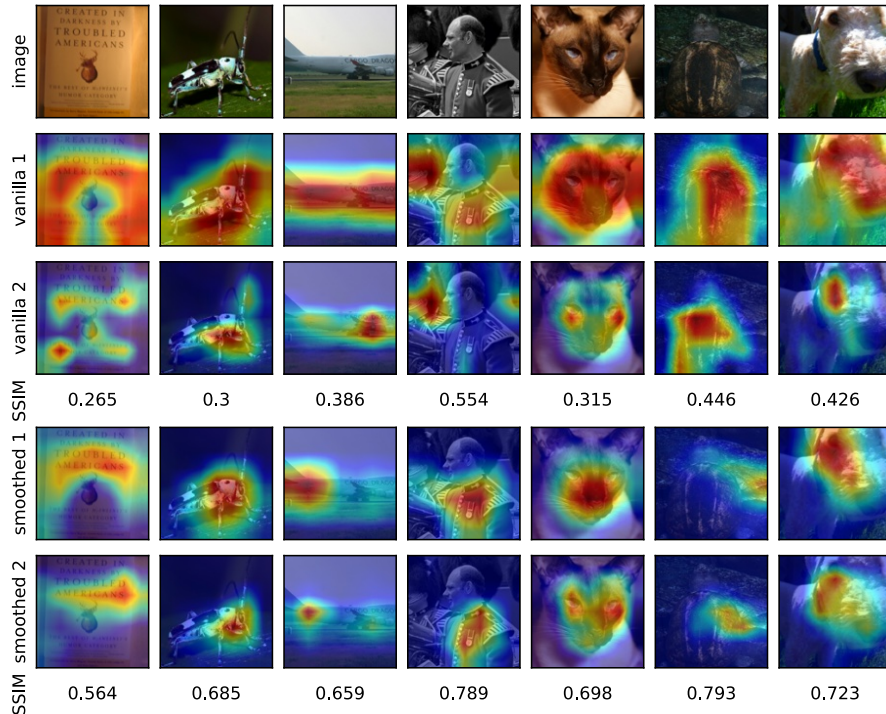


Figure 14: Visualization of Grad-CAM and smoothed version of Grad-CAM differences on ImageNet, where the two neural networks are different pre-trained ResNet50 checkpoints provided by TorchVision (maintainers and contributors, 2016). The first row is the input image. The second and third rows are Simple-Grad results. The fourth and fifth rows are Smooth-Grad with $\sigma/(x_{\max} - x_{\min}) = 0.15$.

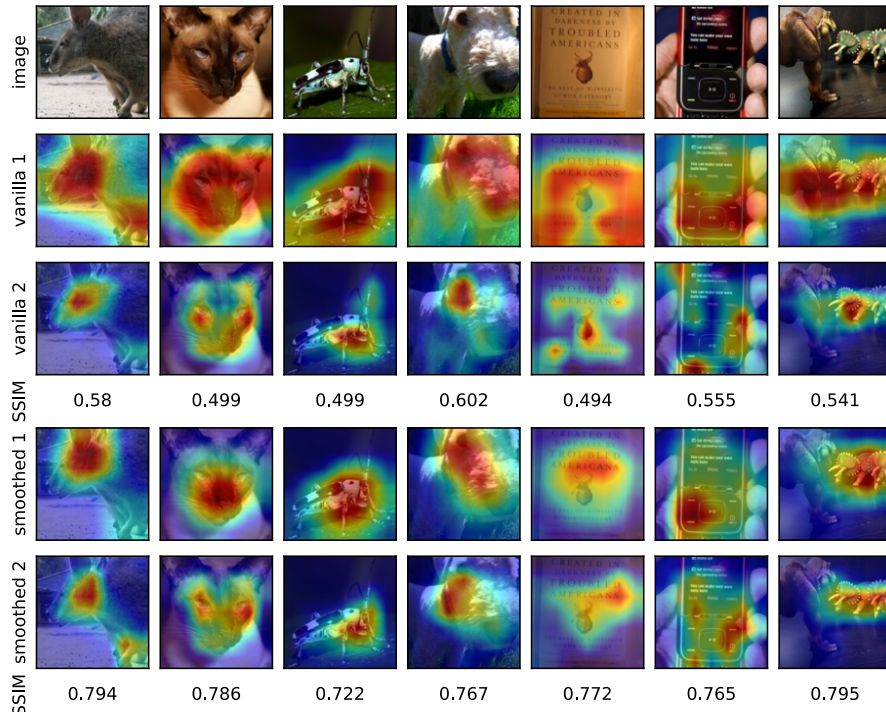


Figure 15: Visualization of Grad-CAM++ and smoothed version of Grad-CAM++ differences on ImageNet, where the two neural networks are different pre-trained ResNet50 checkpoints provided by TorchVision (maintainers and contributors, 2016). The first row is the input image. The second and third rows are Simple-Grad results. The fourth and fifth rows are Smooth-Grad with $\sigma/(x_{\max} - x_{\min}) = 0.15$.

Table 2: Average SSIM and top-k mIoU scores for saliency maps from two neural networks evaluated on a random subset of the ImageNet test set. The two ResNet50 networks are trained on two different splits of the training set. Smoothed scores are computed after applying Gaussian smoothing to both saliency maps.

Algorithm	SSIM	Smoothed SSIM	top-k mIoU	Smoothed top-k mIoU
Gradient \odot Input	0.264	0.323	0.092	0.154
MoreauGrad	0.621	0.785	0.118	0.156

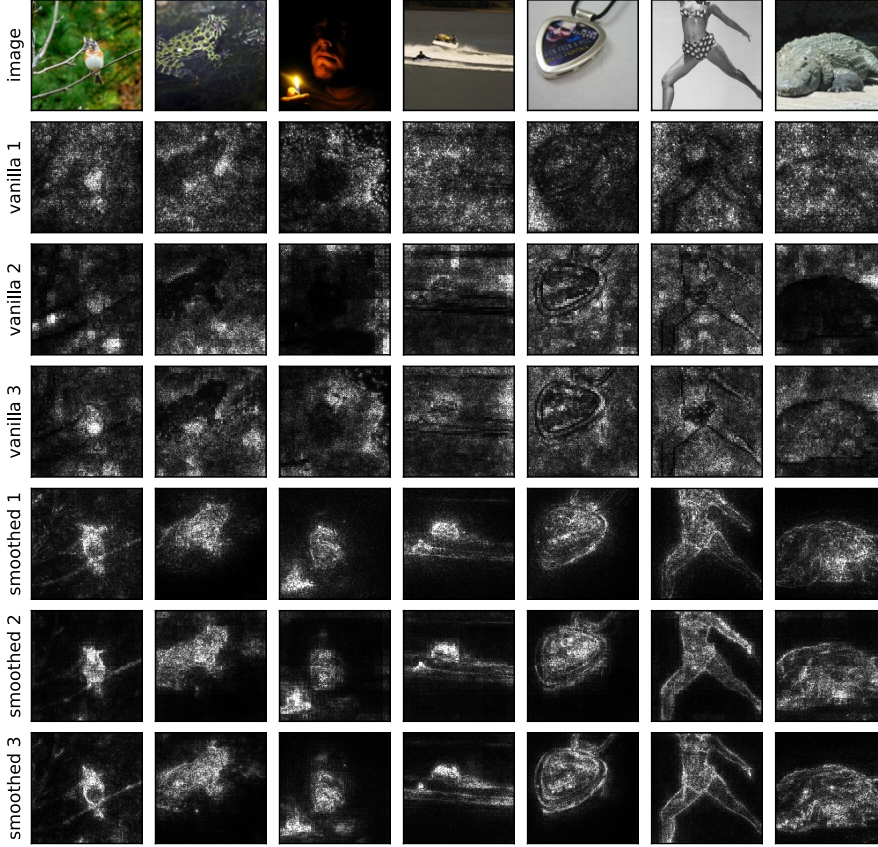


Figure 16: Visualization of Simple-Grad and Smooth-Grad differences on ImageNet, where the three neural networks are pre-trained ResNet50, Swin-T, and ConvNeXt-tiny checkpoints provided by TorchVision (maintainers and contributors, 2016). The first row is the input image. The second, third, and fourth rows are Simple-Grad results. The fifth, sixth, and seventh rows are Smooth-Grad with $\sigma/(x_{\max} - x_{\min}) = 0.15$.

In addition to Table 1 in the main text, we consider two more saliency map algorithms Gradient \odot Input (Shrikumar et al., 2017) and MoreauGrad (Zhang and Farnia, 2023) in Table 2 and can see the stabilizing effect of Gaussian smoothing still holds.

B Bias-Variance Relation

To make our study more comprehensive, we also explore the bias-variance relation after using a smoothing kernel. Intuitively, this relation highly correlates to the stability-fidelity relation we focus on. It is natural to define the ground truth saliency map as the vanilla one without smoothing.

To make the calculation of variance more reliable, we randomly split the training set into ten splits and train ten neural networks independently. Specifically, we define averaged fidelity error as

$$\mathbb{E}_{(x,y) \sim D} \mathbb{E}_{i=1}^{10} \|\mathbb{E}_{z \sim N(0, \sigma^2 I)} \text{Sal}_{A(S_i)}(x + z, y) - \text{Sal}_{A(S_i)}(x, y)\|$$

and define averaged stability error as

$$\mathbb{E}_{(x,y) \sim D} \mathbb{E}_{i=1}^{10} \| \mathbb{E}_{z \sim N(0, \sigma^2 I)} \text{Sal}_{A(S_i)}(x + z, y) - \mathbb{E}_{j=1}^{10} \mathbb{E}_{z \sim N(0, \sigma^2 I)} \text{Sal}_{A(S_j)}(x + z, y) \|^2$$

where $\text{Sal}_{A(S)}(x, y)$ is the non-smoothed saliency map.

See the bias-variance relation figures for both Simple-Grad and Integrated-Grad calculated on ImageNet in Figure 17. The results summarize our results of stability and fidelity and effectively confirm our main results. We can see that smoothing can reduce variance at the cost of bias. We recommend people choose a suitable smoothing σ considering this trade-off in future applications.

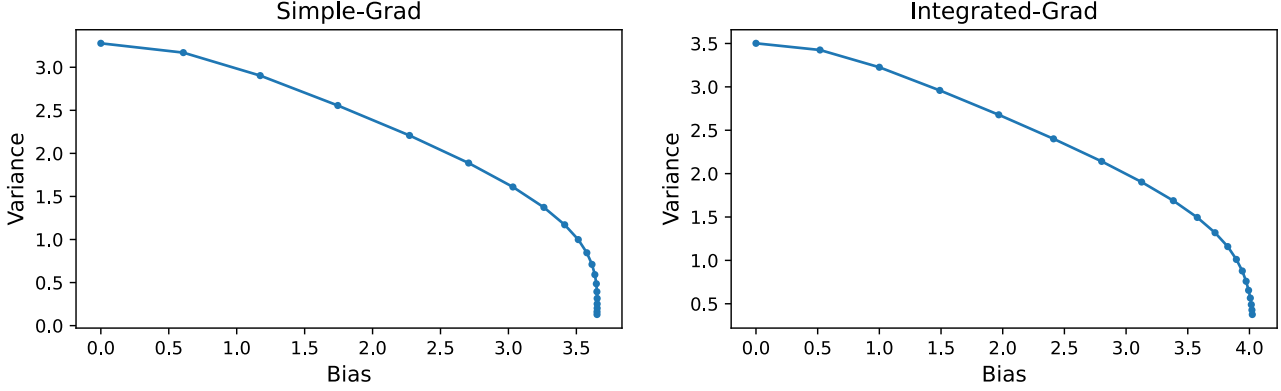


Figure 17: The bias-variance figures for Simple-Grad and Integrated-Grad on ImageNet, by choosing different smoothing factors σ . When choosing a larger σ , bias will increase with variance decreasing. In the figure, the square root of $\sigma/(x_{\max} - x_{\min})$ is sampled from 0 to $\sqrt{0.3}$ with equal intervals.

C More Details of Experiments

C.1 Training Details

For ImageNet, We train 80 epochs using the SGD optimizer with a momentum of 0.9, the StepLR scheduler with a step size of 30 and a gamma of 0.1 to adjust the learning rate, and weight decay of 0.001. We use `RandomResizedCrop` to ensure images have shape 224×224 , and normalize using the mean and standard deviation computed from ImageNet. All these configurations are default ones in the training script provided by Pytorch.² For CIFAR10, we train 100 epochs using the SGD optimizer with a momentum of 0.9, cosine learning rate annealing starting from 0.1 down to 0, and weight decay of 0.001. We normalize images using the mean and standard deviation of 0.5 in all 3 channels. The base models we use are provided by TorchVision (maintainers and contributors, 2016). We run experiments on 4 GeForce RTX 3090 GPUs, the training time for a 500000 training subset takes within 12 hours. Except for the training process, most of our experiments run within one hour.

For each specified number of training data points N , we conduct the experiments three times, using seeds 10007, 5678, and 12345. In each run, the seed is employed to randomly shuffle the list of all indices. We then select the first N indices to train one neural network, and the subsequent N indices to train another. In this way, we can compute standard deviations for Figure 2, 3, 4, 5. For the experiment in 17 which requires 10 splits, we similarly use seed 10007 to shuffle and choose each consecutive N samples as one split.

C.2 Implementation of Saliency Map Algorithms

We use the `saliency` library provided by PAIR³ to compute SimpleGrad, IntegratedGrad, and their smoothed versions, as well as visualize those saliency maps. We use the `pytorch-grad-cam` library⁴ (Gildenblat and

²<https://github.com/pytorch/examples/blob/main/imagenet/main.py>

³<https://github.com/PAIR-code/saliency>

⁴<https://github.com/jacobgil/pytorch-grad-cam>

contributors, 2021) to compute Grad-CAM and Grad-CAM++ since the former library does not natively support them. We set the desired layer to be `model.layer4[-1]` for ResNet50 and `model.norm` for Swin-T, both are close to final layers and our experiments show good visualization results under these choices. According to this library, we visualize a CAM figure as an RGB image by overlaying the cam mask on the image as a heatmap.

When calculating the smoothed version of saliency maps, we draw 100 samples. For IntegratedGrad, we draw 20 intermediate points to compute the integral.

C.3 Other Details

Due to computation speed issues, we choose a 512-sample subset of the whole ImageNet test set to compute results for Table 1 and Figure 6. This test subset is created by randomly shuffling the list of all indices with seed 10007 and choosing the first 512 data points, which remains fixed throughout our experiments.

For the calculation of SSIM, we use the one provided by library `scikit-image`, and set `gaussian_weights` to True, sigma to 1.5, `use_sample_covariance` to False, and specify the `data_range` argument (to 1 for grey images and 255 for RGB images) according to the official suggestions⁵ to match the implementation of (Wang et al., 2004). To calculate top-k mIoU, we set $k = 500$ pixels for both saliency maps, and calculate the average IoU for these pixels with top-k values according to the definition.

D Proofs

D.1 Proof of Proposition 1

We begin by introducing Stein’s lemma, as presented in (Lin et al., 2019). This lemma is crucial to our overall analysis, as it allows us to express the gradient in expectation in a more manageable form.

Lemma D.1. *Stein’s lemma. For a differentiable function f for which the expectation $\mathbb{E}_{z \sim N(0, \sigma^2 I)}[\nabla_x f(x + z)]$ exists, we have*

$$\mathbb{E}_{z \sim N(0, \sigma^2 I)}[\nabla_x f(x + z)] = \mathbb{E}_{z \sim N(0, \sigma^2 I)}\left[\frac{z}{\sigma^2} f(x + z)\right]$$

Lemma D.2. *Suppose function $f : \mathcal{X} \rightarrow \mathcal{Y}$ is L -Lipschitz, then its σ -Gaussian smoothed version \tilde{f} defined by $\tilde{f}(x) = \mathbb{E}_{z \sim N(0, \sigma^2 I)}[f(x + z)]$ is $\frac{L}{\sigma}$ -smooth.*

Proof. Note that L -Lipschitz implies $\|\nabla f(x)\| \leq L$. Define $\tilde{g}(x) = \nabla_x \tilde{f}(x)$. Then for any x_1, x_2 , we have

$$\begin{aligned} \|\tilde{g}(x_1) - \tilde{g}(x_2)\| &\leq \|\mathbb{E}_{z \sim N(0, \sigma^2 I)}[\nabla_x f(x_1 + z)] - \mathbb{E}_{z \sim N(0, \sigma^2 I)}[\nabla_x f(x_2 + z)]\| \\ &= \left\| \mathbb{E}_{z \sim N(0, \sigma^2 I)}\left[\frac{z}{\sigma^2}(f(x_1 + z) - f(x_2 + z))\right] \right\| \\ &= \max_{\|u\|=1} \mathbb{E}_{z \sim N(0, \sigma^2 I)}\left[\frac{u^T z}{\sigma^2}(f(x_1 + z) - f(x_2 + z))\right] \\ &\leq \max_{\|u\|=1} \sqrt{\mathbb{E}_{z \sim N(0, \sigma^2 I)}\left(\frac{u^T z}{\sigma^2}\right)^2 \mathbb{E}_{z \sim N(0, \sigma^2 I)}(f(x_1 + z) - f(x_2 + z))^2} \\ &\leq \frac{1}{\sigma} L \|x_1 - x_2\| \end{aligned}$$

where the second inequality is due to Cauchy-Schwarz inequality. Thus $\tilde{g}(x)$ is $\frac{L}{\sigma}$ -Lipschitz, directly implying $\tilde{f}(x)$ is $\frac{L}{\sigma}$ -smooth. \square

D.2 Proof of Theorem 2

Let $S = (z_1, \dots, z_n)$ and $S' = (z'_1, \dots, z'_n)$ be independent random samples and $S^{(i)} = (z_1, \dots, z_{i-1}, z'_i, z_{i+1}, \dots, z_n)$ be identical to S except the the i -th position. Then we have

⁵https://scikit-image.org/docs/stable/api/skimage.metrics.html#skimage.metrics.structural_similarity

$$\begin{aligned}
\mathbb{E}_{S,A}[L'_S(A(S))] &= \mathbb{E}_{S,A}\left[\frac{1}{n} \sum_{i=1}^n \ell'(A(S), x_i, y_i)\right] \\
&= \mathbb{E}_{S,S',A}\left[\frac{1}{n} \sum_{i=1}^n \ell'(A(S^{(i)}), x'_i, y'_i)\right] \\
&= \mathbb{E}_{S,S',A}\left[\frac{1}{n} \sum_{i=1}^n \ell'(A(S), x'_i, y'_i)\right] - \delta \\
&= \mathbb{E}_{S,A}[L'_D(A(S))] - \delta
\end{aligned}$$

Then the generalization gap can be written as

$$\begin{aligned}
\delta &= \mathbb{E}_{S,A}[L'_D(A(S)) - L'_S(A(S))] \\
&= \mathbb{E}_{S,S',A}\left[\frac{1}{n} \sum_{i=1}^n \ell'(A(S), x'_i, y'_i) - \ell'(A(S^{(i)}), x'_i, y'_i)\right] \\
&= \mathbb{E}_{S,S',i,A}[\ell'(A(S), x'_i, y'_i) - \ell'(A(S^{(i)}), x'_i, y'_i)]
\end{aligned}$$

By taking supremum over any two datasets S and S' differing at only one data point, we can bound

$$\delta \leq \sup_{S,S',x,y} \mathbb{E}_A[\ell'(A(S), x, y) - \ell'(A(S^{(i)}), x, y)] = \epsilon_{\text{stability}}.$$

□

D.3 Upper Bound of Stability Error for Arbitrary Loss Function

Throughout the Appendix, we use $f_{\mathcal{W}}^k(x)$ to denote the neural network function function of the first k layers at input x .

Lemma D.3. *For the class of k -layer neural networks $f_{\mathcal{W}}(x) = W_k \phi(W_{k-1} \phi(\dots \phi(W_1 x))) \in \mathbb{R}^c$ with 1-Lipschitz ϕ where $\phi(0) = 0$, we have*

$$\|f_{\mathcal{W}}(x)\| \leq \Delta_{k,0} C$$

Proof. By the 1-Lipschitz property of the activation function, we have

$$\begin{aligned}
\|f_{\mathcal{W}}^k(x)\| &= \|W_k \phi(W_{k-1} \phi(\dots \phi(W_1 x)))\| \\
&\leq B_k \|W_{k-1} \phi(W_{k-2} \phi(\dots \phi(W_1 x)))\| \\
&= B_k \|f_{\mathcal{W}}^{k-1}(x)\|.
\end{aligned}$$

Since we have $f_{\mathcal{W}}^1(x) \leq B_1 \|x\| \leq B_1 C$, we immediately have the conclusion by induction. □

Lemma D.4. *For the class of k -layer neural networks $f_{\mathcal{W}}(x) = W_k \phi(W_{k-1} \phi(\dots \phi(W_1 x))) \in \mathbb{R}^c$ with 1-Lipschitz ϕ where $\phi(0) = 0$, we have*

$$\text{lip}_{\mathcal{W}}(f_{\mathcal{W}}(x)) \leq \Delta_{k,1} C$$

Proof. Consider the value difference at \mathcal{W} and $\mathcal{W} + \mathcal{V}$. It is bounded by

$$\begin{aligned}
 & \|f_{\mathcal{W}}^k(x) - f_{\mathcal{W}+\mathcal{V}}^k(x)\| \\
 &= \|W_k \phi(f_{\mathcal{W}}^{k-1}(x)) - (W_k + V_k) \phi(f_{\mathcal{W}+\mathcal{V}}^{k-1}(x))\| \\
 &\leq \|W_k \phi(f_{\mathcal{W}}^{k-1}(x)) - (W_k + V_k) \phi(f_{\mathcal{W}}^{k-1}(x))\| \\
 &\quad + \|(W_k + V_k) \phi(f_{\mathcal{W}}^{k-1}(x)) - (W_k + V_k) \phi(f_{\mathcal{W}+\mathcal{V}}^{k-1}(x))\| \\
 &\leq \|V_k\| \cdot \|\phi(f_{\mathcal{W}}^{k-1}(x))\| + \|W_k + V_k\| \cdot \|\phi(f_{\mathcal{W}}^{k-1}(x)) - \phi(f_{\mathcal{W}+\mathcal{V}}^{k-1}(x))\| \\
 &\leq \|\mathcal{V}\| \cdot \|f_{\mathcal{W}}^{k-1}(x)\| + B_k \cdot \text{lip}_{\mathcal{W}}(f_{\mathcal{W}}^{k-1}(x)) \|\mathcal{V}\| \\
 &\leq \left(\prod_{i=1}^{k-1} B_i C + B_k \text{lip}_{\mathcal{W}}(f_{\mathcal{W}}^{k-1}(x)) \right) \|\mathcal{V}\|,
 \end{aligned}$$

where in the last line we apply lemma D.3. It is easy to show $\text{lip}_{\mathcal{W}}(f_{\mathcal{W}}^1(x)) \leq C$, so by induction we have

$$\begin{aligned}
 \text{lip}_{\mathcal{W}}(f_{\mathcal{W}}^k(x)) &\leq \prod_{i=1}^{k-1} B_i C + B_k \text{lip}_{\mathcal{W}}(f_{\mathcal{W}}^{k-1}(x)) \\
 &\leq \sum_{i=1}^k \prod_{j \leq k, j \neq i} B_j C \\
 &= \Delta_{k,1} C.
 \end{aligned}$$

□

To prepare for our next lemma, which involves taking the gradient with respect to \mathcal{W} , we present the following useful result.

Lemma D.5. *For any matrix $W \in \mathbb{R}^{n \times m}$ and vector $x \in \mathbb{R}^c$, we have*

$$\left\| \frac{\partial Wx}{\partial \text{vec}(W)} \right\| = \|x\|$$

Proof. We can write the gradient as

$$\frac{\partial Wx}{\partial \text{vec}(W)} = x^T \otimes I_m.$$

Since the norm of a Kronecker product is the product of the norms of the factors, we immediately have the desired conclusion. □

Lemma D.6. *For the class of k -layer neural networks $f_{\mathcal{W}}(x) = W_k \phi(W_{k-1} \phi(\dots \phi(W_1 x))) \in \mathbb{R}^c$ with 1-Lipschitz activation ϕ where $\phi(0) = 0$, we have*

$$\|\nabla_{\mathcal{W}} f_{\mathcal{W}}^k(x)\| \leq \Delta_{k,1} C$$

Proof. The idea is to tackle the whole parameters into two parts inductively. We have

$$\begin{aligned}
 \|\nabla_{\mathcal{W}_{1..k}} f_{\mathcal{W}}^k(x)\| &\leq \|\nabla_{\mathcal{W}_{1..k-1}} f_{\mathcal{W}}^k(x)\| + \|\nabla_{\mathcal{W}_k} f_{\mathcal{W}}^k(x)\| \\
 &\leq \|W_k \text{diag}(\phi'(f_{\mathcal{W}}^{k-1}(x))) \nabla_{\mathcal{W}_{1..k-1}} f_{\mathcal{W}}^{k-1}(x)\| + \|\phi(f_{\mathcal{W}}^{k-1}(x))\| \\
 &\leq B_k \|\nabla_{\mathcal{W}_{1..k-1}} f_{\mathcal{W}}^{k-1}(x)\| + \|f_{\mathcal{W}}^{k-1}(x)\| \\
 &\leq B_k \|\nabla_{\mathcal{W}_{1..k-1}} f_{\mathcal{W}}^{k-1}(x)\| + \prod_{i=1}^{k-1} B_i C,
 \end{aligned}$$

where in the last inequality we apply lemma D.3. Since $\|\nabla_{\mathcal{W}_1} f_{\mathcal{W}}^1(x)\| \leq \|x\| \leq C$, we can show by induction that

$$\begin{aligned}\|\nabla_{\mathcal{W}_{1..k}} f_{\mathcal{W}}^k(x)\| &\leq \sum_{i=1}^k \prod_{j=i+1}^k B_j \prod_{j=1}^{i-1} B_j C \\ &= \sum_{i=1}^k \prod_{j \leq k, j \neq i} B_j C \\ &= \Delta_{k,1} C.\end{aligned}$$

□

Lemma D.7. For the class of k -layer neural networks $f_{\mathcal{W}}(x) = W_k \phi(W_{k-1} \phi(\dots \phi(W_1 x))) \in \mathbb{R}^c$ with 1-Lipschitz, 1-smooth activation ϕ where $\phi(0) = 0$, under a mild assumption that $B_i, C \geq 1$, we have

$$\text{lip}_{\mathcal{W}}(\nabla_{\mathcal{W}} f_{\mathcal{W}}^k(x)) \leq 3k\Delta_{k,1}^2 C^2$$

Proof. The overall gradient is the concatenation of two parts $\nabla_{\mathcal{W}_{1..k-1}} f_{\mathcal{W}}^k(x)$ and $\nabla_{\mathcal{W}_k} f_{\mathcal{W}}^k(x)$, and we bound the ℓ_2 -norm of points \mathcal{W} and $\mathcal{W} + \mathcal{V}$ for each of the two parts.

To bound the first one, we have

$$\begin{aligned}&\|\nabla_{\mathcal{W}_{1..k-1}} f_{\mathcal{W}}^k(x) - \nabla_{\mathcal{W}_{1..k-1}} f_{\mathcal{W}+\mathcal{V}}^k(x)\| \\ &= \|W_k \text{diag}(\phi'(f_{\mathcal{W}}^{k-1}(x))) \nabla_{\mathcal{W}_{1..k-1}} f_{\mathcal{W}}^{k-1}(x) - (W_k + V_k) \text{diag}(\phi'(f_{\mathcal{W}+\mathcal{V}}^{k-1}(x))) \nabla_{\mathcal{W}_{1..k-1}} f_{\mathcal{W}+\mathcal{V}}^{k-1}(x)\| \\ &\leq \|W_k \text{diag}(\phi'(f_{\mathcal{W}}^{k-1}(x))) \nabla_{\mathcal{W}_{1..k-1}} f_{\mathcal{W}}^{k-1}(x) - (W_k + V_k) \text{diag}(\phi'(f_{\mathcal{W}}^{k-1}(x))) \nabla_{\mathcal{W}_{1..k-1}} f_{\mathcal{W}}^{k-1}(x)\| \\ &\quad + \|(W_k + V_k) \text{diag}(\phi'(f_{\mathcal{W}}^{k-1}(x))) \nabla_{\mathcal{W}_{1..k-1}} f_{\mathcal{W}}^{k-1}(x) \\ &\quad - (W_k + V_k) \text{diag}(\phi'(f_{\mathcal{W}+\mathcal{V}}^{k-1}(x))) \nabla_{\mathcal{W}_{1..k-1}} f_{\mathcal{W}}^{k-1}(x)\| \\ &\quad + \|(W_k + V_k) \text{diag}(\phi'(f_{\mathcal{W}+\mathcal{V}}^{k-1}(x))) \nabla_{\mathcal{W}_{1..k-1}} f_{\mathcal{W}}^{k-1}(x) \\ &\quad - (W_k + V_k) \text{diag}(\phi'(f_{\mathcal{W}+\mathcal{V}}^{k-1}(x))) \nabla_{\mathcal{W}_{1..k-1}} f_{\mathcal{W}+\mathcal{V}}^{k-1}(x)\| \\ &\leq \|\mathcal{V}\| \cdot \|\nabla_{\mathcal{W}_{1..k-1}} f_{\mathcal{W}}^{k-1}(x)\| + B_k \|f_{\mathcal{W}}^{k-1}(x) - f_{\mathcal{W}+\mathcal{V}}^{k-1}(x)\| \cdot \|\nabla_{\mathcal{W}_{1..k-1}} f_{\mathcal{W}}^{k-1}(x)\| \\ &\quad + B_k \|\nabla_{\mathcal{W}_{1..k-1}} f_{\mathcal{W}}^{k-1}(x) - \nabla_{\mathcal{W}_{1..k-1}} f_{\mathcal{W}+\mathcal{V}}^{k-1}(x)\| \\ &\leq \|\mathcal{V}\| \cdot (\Delta_{k-1,1} C + B_k \Delta_{k-1,1}^2 C^2 + B_k \text{lip}_{\mathcal{W}}(\nabla_{\mathcal{W}_{1..k-1}} f_{\mathcal{W}}^{k-1}(x)))\end{aligned}$$

where the last line applies lemma D.4 and lemma D.6. For the second one, we have

$$\begin{aligned}\|\nabla_{\mathcal{W}_k} f_{\mathcal{W}}^k(x) - \nabla_{\mathcal{W}_k} f_{\mathcal{W}+\mathcal{V}}^k(x)\| &= \|\phi(f_{\mathcal{W}}^{k-1}(x)) - \phi(f_{\mathcal{W}+\mathcal{V}}^{k-1}(x))\| \\ &\leq \text{lip}_{\mathcal{W}}(f_{\mathcal{W}}^{k-1}(x)) \|\mathcal{V}\| \\ &\leq \Delta_{k-1,1} C \|\mathcal{V}\| \quad (\text{applying lemma D.4})\end{aligned}$$

Combining these, we have

$$\begin{aligned}\text{lip}_{\mathcal{W}}(\nabla_{\mathcal{W}_{1..k}} f_{\mathcal{W}}^k(x)) &\leq 2\Delta_{k-1,1} C + B_k \Delta_{k-1,1}^2 C^2 + B_k \text{lip}_{\mathcal{W}}(\nabla_{\mathcal{W}_{1..k-1}} f_{\mathcal{W}}^{k-1}(x)) \\ &\leq 3B_k \Delta_{k-1,1}^2 C^2 + B_k \text{lip}_{\mathcal{W}}(\nabla_{\mathcal{W}_{1..k-1}} f_{\mathcal{W}}^{k-1}(x)) \\ &\leq 3 \sum_{i=1}^k \prod_{j=i}^k B_j \Delta_{i-1,1}^2 C^2 \\ &\leq 3 \sum_{i=1}^k \left(\prod_{j=i+1}^k B_j \Delta_{i-1,1} \right) (B_i \Delta_{i-1,1}) C^2 \\ &\leq 3 \sum_{i=1}^k \Delta_{k,1}^2 C^2 \\ &= 3k\Delta_{k,1}^2 C^2\end{aligned}$$

□

Building on previous lemmas, we can now show that the training loss function is Lipschitz and smooth.

Lemma D.8. *Consider the class of k -layer neural networks $f_{\mathcal{W}}(x) = W_k \phi(W_{k-1} \phi(\dots \phi(W_1 x))) \in \mathbb{R}^c$ with 1-Lipschitz activation function ϕ where $\phi(0) = 0$. Assume that $B_i, C \geq 1$. Also, let the training loss for prediction logits $\ell : (\mathbb{R}^c, \mathcal{Y}) \rightarrow \mathbb{R}$ be 1-Lipschitz for all $y \in \mathcal{Y}$. Then our loss function $\ell(f_{\mathcal{W}}(x), y)$ is L -Lipschitz for all x, y . If additionally $\phi(\cdot)$ is 1-smooth and $\ell(\cdot, y)$ is also 1-smooth, then we can show the loss function is β -smooth for all x, y . Here $L \leq \Delta_{k,1} C, \beta \leq (3k + 1)\Delta_{k,1}^2 C^2$.*

Proof. Since ℓ is 1-Lipschitz, due to lemma D.4, we immediately have

$$\text{lip}_{\mathcal{W}}(\ell(f_{\mathcal{W}}(x), y)) \leq \text{lip}_{\mathcal{W}}(f_{\mathcal{W}}(x)) \leq \Delta_{k,1} C.$$

According to the chain rule and smoothness properties, for all x, y , we have

$$\begin{aligned} \text{lip}_{\mathcal{W}}(\nabla_{\mathcal{W}} \ell(f_{\mathcal{W}}(x), y)) &= \text{lip}_{\mathcal{W}}(\nabla \ell(f_{\mathcal{W}}(x), y) \cdot \nabla_{\mathcal{W}} f_{\mathcal{W}}(x)) \\ &\leq \sup_{\mathcal{W}} \|\nabla \ell(f_{\mathcal{W}}(x), y)\| \cdot \text{lip}_{\mathcal{W}}(\nabla_{\mathcal{W}} f_{\mathcal{W}}(x)) + \text{lip}_{\mathcal{W}}(\nabla \ell(f_{\mathcal{W}}(x), y)) \cdot \sup_{\mathcal{W}} \|\nabla_{\mathcal{W}} f_{\mathcal{W}}(x)\| \\ &\leq \text{lip}_{\mathcal{W}}(\nabla_{\mathcal{W}} f_{\mathcal{W}}(x)) + \text{lip}_{\mathcal{W}}(f_{\mathcal{W}}(x))^2 \\ &\leq 3k\Delta_{k,1}^2 C^2 + \Delta_{k,1}^2 C^2 \\ &\leq (3k + 1)\Delta_{k,1}^2 C^2 \end{aligned}$$

Thus, with additional smoothness assumptions, $\ell(f_{\mathcal{W}}(x), y)$ is β -smooth with $\beta = (3k + 1)\Delta_{k,1}^2 C^2$. \square

Next, we quote the results from (Nesterov, 2014) showing that each SGD step will not make two different parameters much more divergent.

Lemma D.9. *Assume the function f is β -smooth. The SGD update rule using f is $w_{t+1} = w_t - \alpha \nabla f(w_t)$. Then, we have*

(a) *For all w_t and w'_t , we can bound*

$$\|w_{t+1} - w'_{t+1}\| \leq (1 + \alpha\beta) \|w_t - w'_t\|$$

(b) *Assume f is additionally convex. Then for any $\alpha \leq 2/\beta$, the following property holds for all w_t and w'_t :*

$$\|w_{t+1} - w'_{t+1}\| \leq \|w_t - w'_t\|$$

After all these previous results, our next lemma proves the upper bounds for the stability of saliency maps under two different assumptions of the loss function. This proof refers to some analysis in (Hardt et al., 2016).

We first state the setting of this lemma. Consider two training sets S and S' of size n that differ at only one data point and we want to show how different the two saliency map losses will become if performing SGD algorithms on the two training sets.

Lemma D.10. *Suppose the training loss function $\ell(f_{\mathcal{W}}(x), y)$ is L -Lipschitz, β -smooth for all x, y . If we run SGD for T steps with a decaying step size $\alpha_t \leq c/t$ in iteration t , then we can bound the stability error of Sal with L' -Lipschitz and M' -bounded corresponding saliency map loss by*

$$\epsilon_{\text{stability}}(\text{Sal}) \leq \frac{1 + \beta c}{n - 1} (2cLL')^{\frac{1}{\beta c + 1}} (TM')^{\frac{\beta c}{\beta c + 1}}$$

Suppose the loss function is additionally convex and the step sizes satisfy $\alpha_t \leq 2/\beta$, then we further have

$$\epsilon_{\text{stability}}(\text{Sal}) \leq \frac{2LL'}{n} \sum_{t=1}^T \alpha_t$$

Proof. To derive a non-trivial upper bound, we note that typically it will take some time before the two SGD trajectories start to diverge. Using this idea, for any time step t_0 , denote the event A as whether $\delta_{t_0} = 0$. If we randomly choose a sample in each iteration, we can show $P(A^c) = 1 - (1 - 1/n)^{t_0} \leq \frac{t_0}{n}$. If we instead iterate the samples in the order of a random permutation, $P(A^c) \leq \frac{t_0}{n}$. Then we have

$$\begin{aligned} & \mathbb{E}[\ell'(w_T, x, y) - \ell'(w'_T, x, y)] \\ &= P(A) \cdot \mathbb{E}[\ell'(w_T, x, y) - \ell'(w'_T, x, y) \mid A] + P(A^c) \cdot \mathbb{E}[\ell'(w_T, x, y) - \ell'(w'_T, x, y) \mid A^c] \\ &\leq \mathbb{E}[\ell'(w_T, x, y) - \ell'(w'_T, x, y) \mid A] + P(A^c) \cdot \sup_{\mathcal{W}, x, y} \ell'(\mathcal{W}, x, y) \\ &\leq L' \mathbb{E}[\delta_T \mid \delta_{t_0} = 0] + \frac{t_0}{n} M' \end{aligned}$$

Define $\Delta_t = \mathbb{E}[\delta_t \mid \delta_{t_0} = 0]$, we then want to bound Δ_{t+1} in terms of Δ_t . With probability $1 - 1/n$, the chosen sample is the same so the iteration function is also the same. According to lemma D.9, the difference of parameters will multiply by at most $1 + \alpha_t \beta$ after this iteration. With probability $1/n$, we need to upper bound the difference between the two SGD updates, and the bound is

$$\begin{aligned} \|w_{t+1} - w'_{t+1}\| &\leq \|w_t - w'_t\| + \|\alpha_t \ell(f_{x_1}(w_t), y_1)\| + \|\alpha_t \ell(f_{x_2}(w_t), y_2)\| \\ &\leq \|w_t - w'_t\| + 2\alpha_t L \end{aligned}$$

Combining the two cases, we have

$$\begin{aligned} \Delta_{t+1} &\leq (1 - 1/n)(1 + \alpha_t \beta) \Delta_t + \frac{1}{n} \Delta_t + \frac{2\alpha_t L}{n} \\ &\leq (1 + (1 - 1/n)c\beta/t) \Delta_t + \frac{2cL}{tn} \\ &\leq \exp((1 - 1/n)c\beta/t) \Delta_t + \frac{2cL}{tn} \end{aligned}$$

According to calculations in (Hardt et al., 2016), we can bound

$$\Delta_T \leq \frac{2L}{\beta(n-1)} \left(\frac{T}{t_0} \right)^{\beta c}$$

Plugging this into our previous inequality for any t_0 , we have

$$\begin{aligned} \mathbb{E}[\ell'(w_T, x, y) - \ell'(w'_T, x, y)] &\leq \frac{t_0}{n} M' + \frac{2LL'}{\beta(n-1)} \left(\frac{T}{t_0} \right)^{\beta c} \\ &\leq M' \left(\frac{t_0}{n} + \frac{2LL'/M'}{\beta(n-1)} \left(\frac{T}{t_0} \right)^{\beta c} \right) \end{aligned}$$

When choosing

$$t_0 = (2cLL'/M')^{\frac{1}{\beta c+1}} T^{\frac{\beta c}{\beta c+1}},$$

we can get the following satisfying upper bound

$$\begin{aligned} \mathbb{E}[\ell'(w_T, x, y) - \ell'(w'_T, x, y)] &\leq \frac{1 + \beta c}{n-1} (2cLL'/M')^{\frac{1}{\beta c+1}} T^{\frac{\beta c}{\beta c+1}} M' \\ &\leq \frac{1 + \beta c}{n-1} (2cLL')^{\frac{1}{\beta c+1}} (TM')^{\frac{\beta c}{\beta c+1}} \end{aligned}$$

Then we consider the case where the loss function is additionally convex and $\alpha_t \leq 2/\beta$. Define $\delta_t = \|w_t - w'_t\|$ as the parameter difference after t iterations, with $\delta_0 = 0$ originally. Then, we have

$$\mathbb{E}[\ell'(w_t, x, y) - \ell'(w'_t, x, y)] \leq L' \mathbb{E}[\delta_t]$$

and our goal would be to bound $\mathbb{E}[\delta_t]$. We want to bound $\mathbb{E}[\delta_{t+1}]$ using $\mathbb{E}[\delta_t]$ to get an iterative formula. Consider the projected SGD update at time $t + 1$. Since the projection operation does not increase Euclidean distance, we can bypass the operation when deriving an upper bound. With probability $1 - 1/n$, we choose the same data point to compute loss for our two parameters. In this case, the difference of two parameters will not increase due to lemma D.9 and the condition $\alpha_t \leq 2/\beta$. With probability $1/n$ the chosen data points are different. In addition to the bound for the first case, we have an extra term for the difference between the two SGD updates. That is, $\|\alpha \nabla \ell(f_{x_1}(w_t), y_1) - \alpha \nabla \ell(f_{x_2}(w_t), y_2)\| \leq 2\alpha_t L$.

Therefore,

$$\mathbb{E}[\delta_{t+1}] \leq \mathbb{E}[\delta_t] + \frac{2\alpha_t L}{n}$$

Unfolding this formula iteratively, we have

$$\mathbb{E}[\delta_t] \leq \frac{2L}{n} \sum_{t=1}^T \alpha_t.$$

Therefore, $\mathbb{E}[\ell'(w_t, x, y) - \ell'(w'_t, x, y)] \leq \frac{2LL'}{n} \sum_{t=1}^T \alpha_t$ holds for all S, S', x, y so the desired bound holds. \square

D.4 Proof of Theorem 5

Lemma D.11. *For the class of k -layer neural networks $f_{\mathcal{W}}(x) = W_k \phi(W_{k-1} \phi(\dots \phi(W_1 x))) \in \mathbb{R}^c$ with 1-Lipschitz, 1-smooth activation ϕ where $\phi(0) = 0$, we have*

$$\|\text{SimpleGrad}_{A(S)}(x, y)\| \leq \Delta_{k,0}$$

Proof. By the definition of gradient, we have the iteration formula

$$\begin{aligned} \|\nabla_x f_{\mathcal{W}}^k(x)\| &= \|W_k \cdot \text{diag}(\phi'(f_{\mathcal{W}}^{k-1}(x))) \cdot \nabla_x f_{\mathcal{W}}^{k-1}(x)\| \\ &\leq B_k \|\nabla_x f_{\mathcal{W}}^{k-1}(x)\| \end{aligned}$$

We can easily show that when $k = 1$, $\|\nabla_x f_{\mathcal{W}}^1(x)\| = \|W_1\| \leq B_1$. Thus solving the iterative formula gives

$$\|\nabla_x f_{\mathcal{W}}^k(x)\| \leq \prod_{i=1}^k B_i = \Delta_{k,0}$$

\square

Lemma D.12. *For Simple-Grad, the Lipschitz constant with respect to \mathcal{W} is bounded by*

$$\text{lip}_{\mathcal{W}}(\text{SimpleGrad}_{A(S)}(x, y)) \leq 2\Delta_{k,0} \sum_{i=1}^{k-1} \Delta_{i,1} C$$

Proof. Consider the difference at points \mathcal{W} and $\mathcal{W} + \mathcal{V}$.

$$\begin{aligned} &\|\nabla_x f_{\mathcal{W}}(x) - \nabla_x f_{\mathcal{W}+\mathcal{V}}(x)\| \\ &\leq \|W_k \cdot \text{diag}(\phi'(f_{\mathcal{W}}^{k-1}(x))) \nabla_x f_{\mathcal{W}}^{k-1}(x) - (W_k + V_k) \cdot \text{diag}(\phi'(f_{\mathcal{W}+\mathcal{V}}^{k-1}(x))) \nabla_x f_{\mathcal{W}+\mathcal{V}}^{k-1}(x)\| \\ &\leq \|V_k \cdot \text{diag}(\phi'(f_{\mathcal{W}}^{k-1}(x))) \nabla_x f_{\mathcal{W}}^{k-1}(x)\| \\ &\quad + \|(W_k + V_k) \cdot (\text{diag}(\phi'(f_{\mathcal{W}}^{k-1}(x))) - \text{diag}(\phi'(f_{\mathcal{W}+\mathcal{V}}^{k-1}(x)))) \nabla_x f_{\mathcal{W}}^{k-1}(x)\| \\ &\quad + \|(W_k + V_k) \cdot \text{diag}(\phi'(f_{\mathcal{W}+\mathcal{V}}^{k-1}(x))) (\nabla_x f_{\mathcal{W}}^{k-1}(x) - \nabla_x f_{\mathcal{W}+\mathcal{V}}^{k-1}(x))\| \\ &\leq \|\mathcal{V}\| \cdot \|\nabla_x f_{\mathcal{W}}^{k-1}(x)\| + B_k \cdot \text{lip}_{\mathcal{W}}(f_{\mathcal{W}}^{k-1}(x)) \|\mathcal{V}\| \cdot \|\nabla_x f_{\mathcal{W}}^{k-1}(x)\| + B_k \text{lip}_{\mathcal{W}}(\nabla_x f_{\mathcal{W}}^{k-1}(x)) \|\mathcal{V}\| \end{aligned}$$

Thus we have

$$\begin{aligned}
 \text{lip}_{\mathcal{W}}(\nabla_x f_{\mathcal{W}}^k(x)) &\leq \Delta_{k-1,0} + B_k \Delta_{k-1,0} \Delta_{k-1,1} C + B_k \text{lip}_{\mathcal{W}}(\nabla_x f_{\mathcal{W}}^{k-1}(x)) \\
 &\leq 2\Delta_{k,0} \Delta_{k-1,1} C + B_k \text{lip}_{\mathcal{W}}(\nabla_x f_{\mathcal{W}}^{k-1}(x)) \\
 &\leq 2\Delta_{k,0} \sum_{i=1}^{k-1} \Delta_{i,1} C
 \end{aligned}$$

□

Given the above two lemmas, we know the loss function defined by Simple-Grad

$$\ell'(A(S), x, y) = \|\text{SimpleGrad}_{A(S)}(x, y) - \text{SimpleGrad}_{A(D)}(x, y)\|$$

is M' -bounded and L' -Lipschitz, with $M' = 2\Delta_{k,0}$ and $L' = 2\Delta_{k,0} \sum_{i=1}^{k-1} \Delta_{i,1} C$. The first constant is due to triangular inequality and the second one is since

$$\|\ell'(\mathcal{W}, x, y) - \ell'(\mathcal{W} + \mathcal{V}, x, y)\| \leq \|\nabla_x f_{\mathcal{W}}(x) - \nabla_x f_{\mathcal{W} + \mathcal{V}}(x)\|.$$

Applying Lemma D.10 with the M' and L' then proves the theorem. □

D.5 Additional Stability Error Bound for Integrated-Grad

We also provide the following theorem for Integrated-Grad. Even with the integration operation, we cannot give a stability error upper bound better than that of Simple-Grad, due to the element-wise multiplication operation.

Theorem D.1. *(a) Convex Loss* Suppose Assumption 3(a), 3(b), and 3(c) hold. If we run the SGD algorithm with step sizes $\alpha_t \leq 1/\beta$ for T times, we can bound the stability error of Integrated-Grad by

$$\epsilon_{\text{stability}}(\text{IntegratedGrad}) \leq \text{Up}_{SC}(\text{SimpleGrad}) \cdot 2C$$

(b) Non-Convex Loss Suppose Assumption 3(b) and 3(c) hold. If we run SGD for T steps with a decaying step size $\alpha_t \leq c/t$ in iteration t , we can bound the stability error of Integrated-Grad by

$$\epsilon_{\text{stability}}(\text{IntegratedGrad}) \leq \text{Up}_{NC}(\text{SimpleGrad}) \cdot 2C$$

Lemma D.13. For Integrated-Grad, the ℓ_2 -norm of the saliency map is bounded by

$$\|\text{IntegratedGrad}_{A(S)}(x, y)\| \leq 2\Delta_{k,0}C$$

Proof. Given that we can upper bound the norm of an integral by the integral of the norm, we have

$$\begin{aligned}
 \left\| (x - x_0) \odot \int_0^1 \nabla_x(f_{x_0+\alpha(x-x_0)}(\mathcal{W}))_y d\alpha \right\| &\leq \|x - x_0\| \cdot \int_0^1 \|\nabla_x f_{x_0+\alpha(x-x_0)}(\mathcal{W})\| d\alpha \\
 &\leq 2C \sup_{x'} \|\nabla_x f_{\mathcal{W}}(x')\| \\
 &\leq 2\Delta_{k,0}C
 \end{aligned}$$

□

Lemma D.14. For Integrated-Grad, the Lipschitz constant with respect to \mathcal{W} is bounded by

$$\text{lip}_{\mathcal{W}}(\text{IntegratedGrad}_{A(S)}(x, y)) \leq 4\Delta_{k,0} \sum_{i=1}^{k-1} \Delta_{i,1} C^2$$

Proof. We have

$$\begin{aligned}
& \left\| (x - x_0) \odot \int_0^1 \nabla_x (f_{x_0 + \alpha(x-x_0)}(\mathcal{W}))_y d\alpha - (x - x_0) \odot \int_0^1 \nabla_x (f_{x_0 + \alpha(x-x_0)}(\mathcal{W} + \mathcal{V}))_y d\alpha \right\| \\
& \leq \|x - x_0\| \cdot \left\| \int_0^1 (\nabla_x f_{x_0 + \alpha(x-x_0)}(\mathcal{W}) - \nabla_x f_{x_0 + \alpha(x-x_0)}(\mathcal{W} + \mathcal{V})) d\alpha \right\| \\
& \leq 2C \cdot \sup_{x'} \|\nabla_x f_{\mathcal{W}}(x') - \nabla_x f_{\mathcal{W}+\mathcal{V}}(x')\| \\
& \leq 2C \cdot 2\Delta_{k,0} \sum_{i=1}^{k-1} \Delta_{i,1} C \|\mathcal{V}\| \\
& = 4\Delta_{k,0} \sum_{i=1}^{k-1} \Delta_{i,1} C^2 \|\mathcal{V}\|,
\end{aligned}$$

which finishes the proof. \square

Given the above two lemmas, with a similar argument as in section D.4, we know the loss function defined by Integrated-Grad is M' -bounded and L' -Lipschitz, with $M' = 4\Delta_{k,0}C$ and $L' = 4\Delta_{k,0} \sum_{i=1}^{k-1} \Delta_{i,1} C^2$. Applying Lemma D.10 then proves the theorem.

\square

D.6 Proof of Theorem 6

For the proof of Smooth-Grad, we need Stein's lemma (lemma D.1) introduced earlier. In the following lemmas, . We also have the following lemma to bound the expected ℓ_2 -norm of a Gaussian vector.

Lemma D.15. *The average norm of an m -dimensional vector given by a normal distribution is bounded by*

$$\mathbb{E}_{x \sim N(0, \sigma^2 I)} \|x\| \leq \sigma \sqrt{m}.$$

Proof. Note that $\|x\|^2$ is the sum of the squares of m random variables with distributions $N(0, \sigma^2)$. Thus

$$\mathbb{E}_{x \sim N(0, \sigma^2 I)} \|x\|^2 = m \mathbb{E}_{z \sim N(0, \sigma^2)} z^2 = m\sigma^2.$$

According to Jensen's inequality, since $f(x) = \sqrt{x}$ is a concave function, we have

$$\mathbb{E}_{x \sim N(0, \sigma^2 I)} \|x\| = \mathbb{E}_{x \sim N(0, \sigma^2 I)} \sqrt{\|x\|^2} \leq \sqrt{\mathbb{E}_{x \sim N(0, \sigma^2 I)} \|x\|^2} = \sigma \sqrt{m}.$$

\square

Lemma D.16. *For Smooth-Grad, if we additionally normalize the perturbed input $x + z$ so that the norm of the neural network input does not exceed C , the ℓ_2 -norm of the saliency map is bounded by*

$$\|\text{SmoothGrad}_{A(S)}(x, y)\| \leq \Delta_{k,0}$$

Proof. Using the result in Lemma D.11, we have

$$\|\mathbb{E}_{z \sim N(0, \sigma^2 I)} \nabla_x f_{\mathcal{W}}(x + z)\| \leq \mathbb{E}_{z \sim N(0, \sigma^2 I)} \|\nabla_x f_{\mathcal{W}}(x + z)\| \leq \Delta_{k,0}$$

\square

Lemma D.17. *For Smooth-Grad, if we additionally normalize the perturbed input $x + z$ so that the norm of the neural network input does not exceed C , the Lipschitz constant with respect to \mathcal{W} is bounded by*

$$\text{lip}_{\mathcal{W}}(\text{SmoothGrad}_{A(S)}(x, y)) \leq \frac{1}{\sigma} C \Delta_{k,1}$$

Proof. By applying Stein's lemma, we have

$$\begin{aligned}
 & \|\mathbb{E}_{z \sim N(0, \sigma^2 I)} [\nabla_x(f_{\mathcal{W}}(x+z))_y - \nabla_x(f_{\mathcal{W}+\mathcal{V}}(x+z))_y]\| \\
 &= \left\| \mathbb{E}_{z \sim N(0, \sigma^2 I)} \left[\frac{z}{\sigma^2} ((f_{\mathcal{W}}(x+z))_y - (f_{\mathcal{W}+\mathcal{V}}(x+z))_y) \right] \right\| \\
 &= \max_{\|u\|=1} \mathbb{E}_{z \sim N(0, \sigma^2 I)} \left[\frac{u^T z}{\sigma^2} ((f_{\mathcal{W}}(x+z))_y - (f_{\mathcal{W}+\mathcal{V}}(x+z))_y) \right] \\
 &\leq \max_{\|u\|=1} \sqrt{\mathbb{E}_{z \sim N(0, \sigma^2 I)} \left[\left(\frac{u^T z}{\sigma^2} \right)^2 \right] \mathbb{E}_{z \sim N(0, \sigma^2 I)} \left[((f_{\mathcal{W}}(x+z))_y - (f_{\mathcal{W}+\mathcal{V}}(x+z))_y)^2 \right]} \\
 &\leq \frac{1}{\sigma} C \Delta_{k,1} \|\mathcal{V}\|
 \end{aligned}$$

Therefore, we have

$$\text{lip}_{\mathcal{W}}(\text{SmoothGrad}_{A(S)}(x, y)) \leq \frac{1}{\sigma} C \Delta_{k,1}.$$

□

Given the above two lemmas, with a similar argument as in section D.4, we know the loss function defined by Integrated-Grad is M' -bounded and L' -Lipschitz, with $M' = 2\Delta_{k,0}$ and $L' = \frac{1}{\sigma} C \Delta_{k,1}$. Applying Lemma D.10 then proves the theorem. □

D.7 Proof of Proposition 7

Consider Simple-Grad. Denote $\mathcal{W} = A(S)$ for simplicity. For any S, x, y, z , we have

$$\begin{aligned}
 & \|\text{SimpleGrad}_{A(S)}(x+z, y) - \text{SimpleGrad}_{A(S)}(x, y)\| \\
 &\leq \|\nabla_x f_{\mathcal{W}}^k(x) - \nabla_x f_{\mathcal{W}}^k(x+z)\| \\
 &= \|W_k \cdot \text{diag}(\phi'(f_{\mathcal{W}}^{k-1}(x)) \nabla_x f_{\mathcal{W}}^{k-1}(x) - W_k \cdot \text{diag}(\phi'(f_{\mathcal{W}}^{k-1}(x+z)) \nabla_x f_{\mathcal{W}}^{k-1}(x+z))\| \\
 &\leq B_k (\|(\text{diag}(\phi'(f_{\mathcal{W}}^{k-1}(x)) - \text{diag}(\phi'(f_{\mathcal{W}}^{k-1}(x+z))) \nabla_x f_{\mathcal{W}}^{k-1}(x)\| \\
 &\quad + \|\text{diag}(\phi'(f_{\mathcal{W}}^{k-1}(x+z))(\nabla_x f_{\mathcal{W}}^{k-1}(x) - \nabla_x f_{\mathcal{W}}^{k-1}(x+z))\|) \\
 &\leq B_k (\|f_{\mathcal{W}}^{k-1}(x) - f_{\mathcal{W}}^{k-1}(x+z)\| \cdot \|\nabla_x f_{\mathcal{W}}^{k-1}(x)\| + \|\nabla_x f_{\mathcal{W}}^{k-1}(x) - \nabla_x f_{\mathcal{W}}^{k-1}(x+z)\|) \\
 &\leq B_k (\Delta_{k-1,0}^2 \|z\| + \|\nabla_x f_{\mathcal{W}}^{k-1}(x) - \nabla_x f_{\mathcal{W}}^{k-1}(x+z)\|) \\
 &\leq \sum_{i=1}^{k-1} \prod_{j=i+1}^k B_j \Delta_{i,0}^2 \|z\| \\
 &= \Delta_{k,0} \sum_{i=1}^{k-1} \Delta_{i,0} \cdot \|z\|
 \end{aligned}$$

Then we have for any S, x ,

$$\begin{aligned}
 & \mathbb{E}_{z \sim N(0, \sigma^2 I)} \|\text{SimpleGrad}_{A(S)}(x+z, y) - \text{SimpleGrad}_{A(S)}(x, y)\| \\
 &\leq \mathbb{E}_{z \sim N(0, \sigma^2 I)} \left[\Delta_{k,0} \sum_{i=1}^{k-1} \Delta_{i,0} \cdot \|z\| \right] \\
 &\leq \Delta_{k,0} \sum_{i=1}^{k-1} \Delta_{i,0} \sigma \sqrt{m},
 \end{aligned}$$

which implies

$$\epsilon_{\text{fidelity}}(\text{SimpleGrad}) \leq \Delta_{k,0} \sum_{i=1}^{k-1} \Delta_{i,0} \sigma \sqrt{m}.$$

Consider Integrated-Grad. For any S, x, y, z , we have

$$\begin{aligned}
 & \| \text{IntegratedGrad}_{A(S)}(x + z, y) - \text{IntegratedGrad}_{A(S)}(x, y) \| \\
 &= \left\| (x + z - x_0) \odot \int_0^1 \nabla_x(f_{\mathcal{W}}(x_0 + \alpha(x + z - x_0)))_y d\alpha - (x - x_0) \odot \int_0^1 \nabla_x(f_{\mathcal{W}}(x_0 + \alpha(x - x_0)))_y d\alpha \right\| \\
 &\leq \left\| (x + z - x_0) \odot \left(\int_0^1 \nabla_x(f_{\mathcal{W}}(x_0 + \alpha(x + z - x_0)))_y d\alpha - \int_0^1 \nabla_x(f_{\mathcal{W}}(x_0 + \alpha(x - x_0)))_y d\alpha \right) \right\| \\
 &\quad + \left\| (x + z - x_0) \odot \int_0^1 \nabla_x(f_{\mathcal{W}}(x_0 + \alpha(x - x_0)))_y d\alpha - (x - x_0) \odot \int_0^1 \nabla_x(f_{\mathcal{W}}(x_0 + \alpha(x - x_0)))_y d\alpha \right\| \\
 &\leq \|x + z - x_0\| \sup_{\alpha \in [0,1]} \|\nabla_x f_{\mathcal{W}}(x_0 + \alpha(x + z - x_0)) - \nabla_x f_{\mathcal{W}}(x_0 + \alpha(x - x_0))\| \\
 &\quad + \|z\| \sup_{\alpha \in [0,1]} \|\nabla_x f_{\mathcal{W}}(x_0 + \alpha(x - x_0))\| \\
 &\leq \|x + z - x_0\| \cdot \Delta_{k,0} \sum_{i=1}^{k-1} \Delta_{i,0} \min(\|z\|, C) + \|z\| \Delta_{k,0}
 \end{aligned}$$

Then we have for any S, x, y ,

$$\begin{aligned}
 & \mathbb{E}_{z \sim N(0, \sigma^2 I)} \| \text{IntegratedGrad}_{A(S)}(x + z, y) - \text{IntegratedGrad}_{A(S)}(x, y) \| \\
 &\leq \Delta_{k,0} \sum_{i=1}^{k-1} \Delta_{i,0} \mathbb{E}_{z \sim N(0, \sigma^2 I)} [\|x - x_0\| \|z\| + \|z\| C] + \mathbb{E}_{z \sim N(0, \sigma^2 I)} [\|z\| \Delta_{k,0}] \\
 &\leq \Delta_{k,0} \sum_{i=1}^{k-1} \Delta_{i,0} \cdot 3C\sigma\sqrt{m} + \Delta_{k,0}\sigma\sqrt{m} \\
 &\leq \Delta_{k,0} \sum_{i=1}^{k-1} \Delta_{i,0} \sigma\sqrt{m} \left(3C + \frac{1}{\sum_{i=1}^{k-1} \Delta_{i,0}} \right) \\
 &\leq \Delta_{k,0} \sum_{i=1}^{k-1} \Delta_{i,0} \sigma\sqrt{m} (3C + 1),
 \end{aligned}$$

which concludes the second part of our desired theorem, which is

$$\epsilon_{\text{fidelity}}(\text{IntegratedGrad}) \leq \Delta_{k,0} \sum_{i=1}^{k-1} \Delta_{i,0} (3C + 1) \sigma \sqrt{m}.$$

□